S. Meraglia, D. Invernizzi, M. Lovera, T. Mohtar, A. Bursi
Design of an Active Balancing System for Rotating Orbital Devices
Journal of Guidance Control and Dynamics, Vol. 46, N. 12, 2023, p. 2315-2329
doi:10.2514/1.G007385

Design of an active balancing system for rotating orbital devices

Salvatore Meraglia *, Davide Invernizzi †, and Marco Lovera‡
Polytechnic University of Milan, 20156 Milan, Italy

Tharek Mohtar§, and Alessandro Bursi¶
OHB Italia S.p.A., 20151 Milan, Italy

This paper presents the design of an active balancing system for rotating orbital devices, motivated by recent space applications for spacecraft endowed with rotating payloads. The main motivation behind this work is the Copernicus Imaging Microwave Radiometry (CIMR) mission which will feature a large rotating microwave radiometer to provide observations of sea-surface temperature, sea-ice concentration and sea-surface salinity. Due to the presence of highly uncertain inertial asymmetries in the rotating device, potentially large internal forces and torques can appear at interface between the spacecraft and the rotor which can cause a significant degradation of the system performance and can even affect its stability. To counteract such unbalance effects, in this work we develop an active balancing system made of a suitable set of actuated movable masses and sensors. Exploiting the time-periodic nature of the underlying dynamics, a harmonic controller has been designed to command the positions of the actuated masses in such a way that the effects of rotor unbalance are significantly reduced. After extensive numerical simulations, accounting for both parametric uncertainties and exogenous disturbances in the model, a dedicated breadboard has been developed and experimental validation of the control law has been carried out.

Nomenclature

$f_O \in \mathbb{R}^3$	=	interface reaction force, N
$f^e \in \mathbb{R}^3$	=	force associated with environmental effects, N
$h_O \in \mathbb{R}^3$	=	angular momentum, Nm
$J_r \in \mathbb{R}^{3\times3}$	=	inertia matrix of the rotor, kgm^2
$\bar{J}_{i3} \in \mathbb{R}$	=	nominal term of inertia moment, kgm^2
$k \in \mathbb{Z}_{\geq 0}$	=	discrete-time index

*PhD Student, Department of Aerospace Science and Technology, via La Masa, 34; salvatore.meraglia@polimi.it (Corresponding Author).
†Assistant Professor, Department of Aerospace Science and Technology, via La Masa, 34.
‡Full Professor, Department of Aerospace Science and Technology, via La Masa, 34.
§Space Mechanisms Engineer, OHB Italia S.p.A., Via Gallarate 150.
¶Mechanisms Business Unit Manager, OHB Italia S.p.A., Via Gallarate 150.

$m_j \in \mathbb{R}_{>0}$ = mass of the *j-th* balancing mass, kg

$m_p \in \mathbb{R}_{>0}$ = total mass of the payload (rotor plus active blancing system), kg

$m_r \in \mathbb{R}_{>0}$ = mass of the rotor, kg

$N_m \in \mathbb{Z}_{>0}$ = number of movable masses

$n_u \in \mathbb{R}_{>0}$ = number of outputs

$n_y \in \mathbb{R}_{>0}$ = number of inputs

O_i = origin of the inertial frame

O_b = origin of the base-fixed frame

O_a = attachment point between the base and the payload

$Q \in \mathbb{R}^{n_y \times n_y}$ = weighting matrix for plant output in cost function

$q \in \mathbb{R}^3$ = translational momentum, N

$R \in \mathbb{R}^{n_u \times n_u}$ = weighting matrix for control input in cost function

$R_b^i \in \mathrm{SO}(3)$ = rotation matrix describing the attitude of the spacecraft-fixed frame with respect to the inertial frame

$R_r^i \in \mathrm{SO}(3)$ = rotation matrix describing the attitude of the payload-fixed frame with respect to the inertial frame

$R_r^b \in \mathrm{SO}(3)$ = rotation matrix describing the attitude of the rotor-fixed frame with respect to the spacecraft-fixed frame

$s_j \in \mathbb{R}$ = relative displacement of the *j-th* balancing mass, m

$\bar{S}_i \in \mathbb{R}$ = nominal term of static moment, kgm

$\underline{s}_j \in \mathbb{R}$ = lower limit of the *j-th* stroke, m

$\bar{s}_j \in \mathbb{R}$ = upper limit of the *j-th* stroke, m

$T \in \mathbb{R}^{2n_y \times n_u}$ = T-matrix

$u \in \mathbb{R}^{n_u}$ = desired positions of the ABS masses in the rotating frame, m

$v_G^r \in \mathbb{R}^3$ = inertial velocity of the center of mass of the rotor, m/s

$v_O \in \mathbb{R}^3$ = inertial velocity of the attachment point O, m/s

$v_i \in \mathbb{R}^3$ = velocity of the *j-th* mass, m/s

${}^r x_{G_p}^r \in \mathbb{R}^3$ = location of the center of mass of the payload, m

${}^r x_j^r \in \mathbb{R}^3$ = zero location of the *j-th* balancing mass, with respect to O_a expressed in $\mathcal{F}_r$, m

${}^i x_i^i \in \mathbb{R}^3$ = position of the *j-th* balancing mass, with respect to O_i expressed in $\mathcal{F}_i$, m

${}^i x_b^b \in \mathbb{R}^3$ = difference vector between O_b and O_i expressed in $\mathcal{F}_i$, m

${}^r x_G^r \in \mathbb{R}^3$ = difference vector between the rotor CoM G and O_a expressed in $\mathcal{F}_r$, m

$y_1 \in \mathbb{R}^{2n_y}$ = first harmonics of measured outputs

$\Delta J_{i3} \in \mathbb{R}$ = perturbation term of inertia moment, kgm^2

$\Delta S_i \in \mathbb{R}$ = perturbation term of static moment, kgm

$\Delta t \in \mathbb{R}_{>0}$ = time interval between consecutive updates, s

$\tau_O \in \mathbb{R}^3$ = interface reaction torque, Nm

$\tau_O^e \in \mathbb{R}^3$ = torque associated with environmental effects, Nm

${}^r\omega^i \in \mathbb{R}^3$ = payload angular velocity, expressed in $\mathcal{F}_r$, rad/s

${}^b\omega^i \in \mathbb{R}^3$ = (body) angular velocity of the spacecraft base, rad/s

$\Omega \in \mathbb{R}$ = angular rate of the rotor relative to the spacecraft-fixed frame, rad/s

I. INTRODUCTION

Future space missions will increasingly rely on the use of large rotating payloads, in particular in the context of missions requiring high Earth observation capabilities [1, 2]. Accommodation restrictions, whether due to launcher fairing envelopes or limitations and constraints by the spacecraft, make it necessary to stow for launch and deploy in-orbit the payloads that are exceeding these restrictions due to their operational dimensions [3]. These systems require a careful design, because the unbalanced force and moment arising from inertial asymmetries can lead to the reduction of accuracy and stability of the spacecraft attitude and the induced vibrations can directly affect the quality of the collected data. For instance, one of the most challenging aspects of the Soil Moisture Active Passive (SMAP) observatory mission by NASA [1] was the design of the spinning reflector and beam assembly to minimize the impact of the inertial unbalances. Ground testing and characterization of the assembly was evaluated, but was considered impractical. It was determined that a program of detailed analysis and modeling (detailed to the screw, nut, washer and glue-line level) in conjunction with a rigorous hardware mass properties measurement process at the piece parts and sub-assembly level could effectively characterize the inertial properties of the system within the requirements dictated by the spacecraft dynamics [4]. However, the problems associated with unbalancing are magnified when the payload is large and, as a consequence, the operational life could become shorter and the operational reliability could degrade. In worst-case scenarios, the attitude control system may fail to stabilize the spacecraft or the unbalanced loads may damage the motor sustaining the spin motion, thereby undermining the outcome of the mission.

The future Copernicus Imaging Microwave Radiometry (CIMR) mission [5], which aims to provide high spatial resolution microwave radiometry measurements, employs a conical scanning geometry with a spinning antenna reflector rotating about the nadir-pointing axis of the spacecraft to guarantee a high spatio-temporal resolution. The outward appearance of the CIMR spacecraft (see Figure 1 from ESA*) is dominated by a 9-meters large deployable mesh antenna that is mounted on the spun portion of the spacecraft and on the end of a 12-meters long boom. The CIMR payload involves components much larger than the SMAP ones (6-meters large reflector 6-meters long boom [6]) and, as a consequence, even an accurate manufacturing might not guarantee sufficient suppression of the inertial unbalances. For this reason, the effects of the unbalances might have to be corrected at commissioning by means of a dedicated

*https://www.esa.int/ESA_Multimedia/Images/2020/11/CIMR.

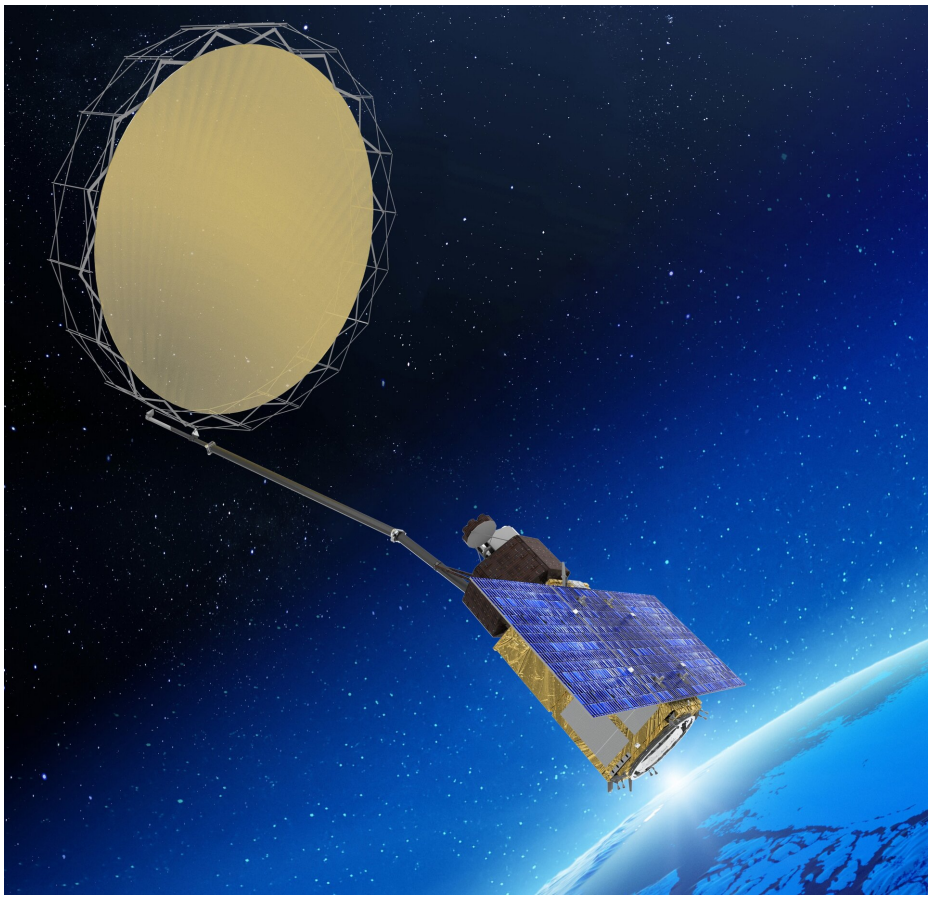

Figure 1 CIMR spacecraft.

balancing system [7].

In this paper, the concept introduced in the preliminary work [8] of an Active Balancing System (short, ABS) to actively counteract unbalance effects in a rotor, is extended here to explore a viable solution to the balancing of the CIMR rotating payload. The original ABS concept has been further analyzed and generalized and then experimentally validated on a simplified breadboard. Inspired by previous work on active balancing [9], the proposed ABS is based on:

- a set of movable masses, mounted on the rotor, and actuated through linear actuators;
- sensors, mounted on the spacecraft base, capable of measuring the components of the in-plane joint force and torque to be canceled;
- an electronic unit with the control system to process data from the sensors and to separately command the actuators to move the balancing masses to the target locations on the strokes.

After a detailed definition of a generic ABS configuration and the derivation of a suitable dynamical model, an analytical framework useful for the analysis of the system balancing capabilities is proposed. The proposed approach assumes a decoupled control architecture, wherein the attitude of the spacecraft is controlled through the actuators of the spacecraft base while the ABS controller tries to cancel out the effects of inertial unbalances in the rotor by moving the masses at

suitable locations. In this regard, it has been recently shown in [10] that a properly tuned PD-like controller is capable of keeping a stable attitude in the presence of inertial unbalances in the rotating device and ensures convergence to the desired attitude for vanishing unbalances, thereby allowing for balancing operations to be carried out safely. In this work, assuming that the spacecraft controller keeps the attitude close to the desired one, we show that through suitable assumptions the rotating device can be considered as fixed on the ground when designing the control algorithm of the ABS. One of the main contribution of this work lies in showing that the complex payload dynamics can be approximated by a perturbed LTP system, thanks to the use of sensors placed on the (non-rotating) spacecraft base, where the main source of perturbation is associated with the rotor unbalances. The disturbance rejection problem for such systems can be addressed using harmonic control theory, which has been considered both in the context of helicopter vibration reduction [11, 12] and rotor balancing [13–16]. Specifically, in this work we exploit a robust harmonic control law borrowed from [17] to counteract model uncertainty issues resulting from the adopted approximations.

A multi-body model of the rotor with the ABS system has been developed to evaluate the stability and performance of the proposed design in a sufficiently accurate simulation environment, replicating possible effects coming from the space environment, and to tune the control law. A Monte Carlo analysis has been carried out to assess the behavior of the system when accounting also for parametric uncertainties and exogenous disturbances. In order to check the effectiveness of the proposed design, a breadboard consisting of a single-plane ABS with the possibility of adding artificial unbalances has been designed and built. In the final part of the paper, experimental results obtained on the breadboard are reported to show that the proposed ABS is capable of reducing the unbalance effects, namely, the force and torque at the interface point, within required admissible levels.

II. Notation

$\mathbb{R}$ ($\mathbb{R}_{>0}, \mathbb{R}_{\geq 0}$) denotes the set of (positive, non-negative) real numbers, $\mathbb{Z}_{\geq 0}$ denotes the set of non-negative integers, $\mathbb{R}^n$ denotes the n-dimensional Euclidean space and $\mathbb{R}^{m\times n}$ the set of $m \times n$ real matrices. The i-th vector of the canonical basis in $\mathbb{R}^n$, *i.e.*, the vector with a 1 in the i-th coordinate and 0's elsewhere, is denoted as e_i and the identity matrix in $\mathbb{R}^{n\times n}$ is $I_n := [e_1 \cdots e_i \cdots e_n]$. Given vectors $x, y \in \mathbb{R}^n$, the standard inner product is defined as $\langle x, y\rangle := x^\top y$. The Euclidean norm of a vector $x \in \mathbb{R}^n$ is $\|x\| := \sqrt{\langle x, x\rangle}$. The n-dimensional unit sphere is denoted as $\mathbb{S}^n := \{x \in \mathbb{R}^{n+1} : \|x\| = 1\}$. A Cartesian reference frame is the defined as $\mathcal{F}_a := (O_a, \{a_1, a_2, a_3\})$, where O_a represents the origin and $a_i \in \mathbb{S}^2$, $i = 1, 2, 3$, are three mutually orthogonal unit axis defining a right-handed triad. We use the notation ${}^a x$ to denote the components of a free vector x expressed in frame $\mathcal{F}_a$, whereas ${}^b x_P^a = ({}^b x_{P,1}^a, {}^b x_{P,2}^a, {}^b x_{P,3}^a)$ to represent the components of the position vector $\overrightarrow{O_a P}$ expressed in frame $\mathcal{F}_b$. The set $\mathrm{SO}(3) := \{R \in \mathbb{R}^{3\times 3} : R^\top R = I_3, \det(R) = 1\}$ denotes the three-dimensional Special Orthogonal group. The notation R_b^a is used to denote the rotation matrix that transforms the components of a vector from frame b to frame a, which is defined as $R_b^a := [{}^a b_1 \; {}^a b_2 \; {}^a b_3]$. The angular velocity of frame $\mathcal{F}_b$ with respect to frame $\mathcal{F}_a$, expressed in $\mathcal{F}_b$, is denoted as ${}^b\omega^a$, and is such that $\dot{R}_b^a = R_b^a S({}^b\omega^a)$. Given

$\omega \in \mathbb{R}^3$, the map $S(\cdot) : \mathbb{R}^3 \to \mathfrak{so}(3) := \{\Omega \in \mathbb{R}^{3\times 3} : \Omega = -\Omega^\top\}$ is such that $S(\omega)y = \omega \times y, \ \forall y \in \mathbb{R}^3$, where $\times$ represents the cross product in $\mathbb{R}^3$.

III. ACTIVE BALANCING SYSTEM MODELING AND CONTROL PROBLEM FORMULATION

This section is devoted to presenting the problem addressed in this work. As mentioned in the Introduction, the system under investigation consists of a rotating device, henceforth called “rotor", mounted on a spacecraft, which is referred to as “base". To tackle the undesired effects associated with the inertial unbalance of the rotor, in this work we consider the use of an ABS made of a set of $N_m \in \mathbb{Z}_{>0}$ movable masses, mounted on the rotor, and by sensors, mounted on the spacecraft, capable of measuring the components of the joint force and torque perpendicular to the axis of rotation. The system comprising the rotor and the ABS will be referred to as the “payload" in the following. In deriving the model for control, we consider the system to be made of rigid bodies, under the (reasonable) assumption that the balancing masses are moved slowly enough to avoid exciting the structural dynamics, which are predominately associated with the flexibility of the reflector antenna.

A. Multibody system configuration and kinematics

To characterize the system configuration, several Cartesian reference frames must be introduced (see Figure 2):

- an inertial frame $\mathcal{F}_i := (O_i, \{i_1, i_2, i_3\})$ fixed at center of the Earth;
- a base-fixed frame $\mathcal{F}_b := (O_b, \{b_1, b_2, b_3\})$, with O_b being the CoM of the base;
- a base-fixed frame $\mathcal{F}_a := (O_a, \{a_1, a_2, a_3\})$, with O_a being the attachment point between the base and the payload and $a_3 \in \mathbb{S}^2$ identifying the axis of rotation;
- a payload-fixed frame $\mathcal{F}_r := (O_r, \{r_1, r_2, r_3\})$, with $O_r \equiv O_a =: O$.

  Based on the above description, we are considering (without loss of generality) $a_i \equiv b_i \ \forall i \in \{1, 2, 3\}$, namely, that the frame $\mathcal{F}_a$ is aligned with $\mathcal{F}_b$.

We now proceed by introducing the relevant quantities to describe the kinematics of the system. The attitude of the rotor is represented by the rotation matrix $R_r^i \in \mathrm{SO}(3)$ which is described as a composition of two rotations:

$$R_r^i = R_b^i R_r^b \tag{1}$$

where R_b^i is the rotation matrix describing the attitude of the spacecraft-fixed frame $\mathcal{F}_b$ with respect to the inertial frame

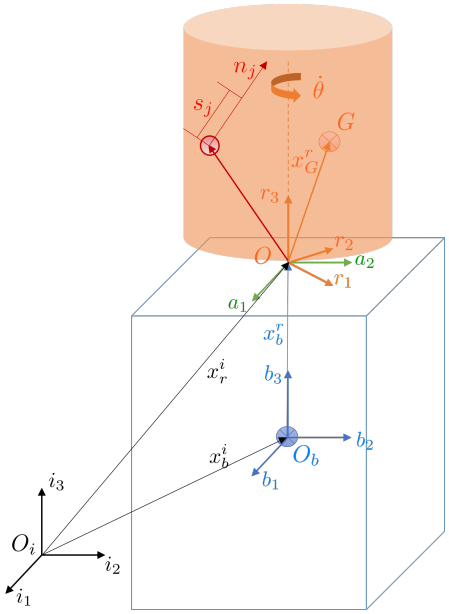

Figure 2 Multibody spacecraft configuration and definition of the reference frames.

$\mathcal{F}_i$ while

$$R_r^b := \begin{bmatrix} \cos(\theta) & -\sin(\theta) & 0 \\ \sin(\theta) & \cos(\theta) & 0 \\ 0 & 0 & 1 \end{bmatrix} \tag{2}$$

is the rotation matrix describing the attitude of the rotor-fixed frame $\mathcal{F}_r$ with respect to the spacecraft-fixed frame $\mathcal{F}_b$, parametrized in terms of the rotation angle $\theta \in [0, 2\pi)$ and the spin axis $e_3 = [\,0\;0\;1\,]^\top$. The position of the *j-th* balancing mass expressed in $\mathcal{F}_i$, denoted by ${}^i x_i^i \in \mathbb{R}^3$, is a function of the corresponding relative displacement $s_j \in \mathbb{R}$ as follows:

$${}^i x_i^i = {}^i x_r^r + r_j(s_j) \tag{3}$$

where $r_j(s_j) := R_r^i({}^r x_j^r + s_j n_j)$, with ${}^r x_j^r := [\,\bar{x}_j\;\bar{y}_j\;\bar{z}_j\,]^\top \in \mathbb{R}^3$ is the zero location (*i.e.*, $s_j = 0$) of the *j-th* balancing mass relative to O and expressed in $\mathcal{F}_r$, while $n_j \in \mathbb{S}^2$ is the unit vector assigning the corresponding displacement direction. As the strokes on which the actuated masses can move have finite length, we define $\underline{s}_j$ and $\bar{s}_j$ the lower and upper limit of the *j-th* stroke, respectively, such that $s_j \in [\underline{s}_j, \bar{s}_j]$.

The attitude kinematics of the rotor can be derived by differentiation of (1):

$$\begin{aligned} \dot{R}_r^i &= \dot{R}_b^i R_r^b + R_b^i \dot{R}_r^b = R_b^i S({}^b\omega^i) R_r^b + R_b^i R_r^b S(e_3)\Omega \\ &= R_b^i R_r^b (R_r^b)^\top S({}^b\omega^i) R_r^b + S(e_3)\Omega) = R_b^i R_r^b S((R_r^b)^\top {}^b\omega^i + \Omega e_3) \end{aligned} \tag{4}$$

where ${}^b\omega^i \in \mathbb{R}^3$ is the (body) angular velocity of the spacecraft base with respect to the inertial frame, $\Omega := \dot{\theta}(t) \in \mathbb{R}$ is the angular rate of the rotor relative to the frame $\mathcal{F}_a$, which is assumed to be constant, *i.e.*, $\dot{\Omega}(t) = \ddot{\Omega}(t) \equiv 0$ $\forall t$. In deriving (4) we exploited the linearity property of the $S^{-1}(\cdot)$ map and the property $S^{-1}(R^\top S(\omega)R) = R^\top\omega$ $\forall (R, \omega) \in \mathrm{SO}(3) \times \mathbb{R}^3$. From equation (4), one can define the payload angular velocity resolved in $\mathcal{F}_r$ as

$$ {}^r\omega^i = R_b^r\, {}^b\omega^i + \Omega e_3, \tag{5} $$

which gives the compact expression $\dot{R}_r^i = R_r^i S({}^r\omega^i)$. The inertial velocity of the center of mass of the rotor (point G in Figure 2) is obtained by differentiating the expression ${}^i x_G^i := {}^i x_r^i + R_r^i\, {}^r x_G^r$, which yields:

$$ {}^i v_G^i = {}^i v_O^i + R_r^i S({}^r\omega^i)\, {}^r x_G^r \tag{6} $$

where ${}^i v_O^i := {}^i \dot{x}_r^i$ denotes the inertial velocity of the attachment point O. The velocity of the *j-th* mass, resolved again in $\mathcal{F}_i$, is given by

$$ {}^i v_j^i = {}^i v_O^i + R_r^i S({}^r\omega^i)({}^r x_j^r + s_j n_j) + R_r^i \dot{s}_j n_j, \tag{7} $$

which comprises contributions from the motion of the attachment point (v_O), the overall angular velocity of the payload (${}^r\omega^i$) and the relative motion of the mass ($\dot{s}_j$).

At this point, all the information needed to characterize the proposed balancing system has been introduced and we can formally define the ABS system.

Definition 1 *Given a rotor-fixed frame $\mathcal{F}_r$, the ABS with N_m movable masses is defined by the tuple* $(m_1, {}^r x_1^r, n_1, \underline{s}_1, \bar{s}_1, \ldots, m_{N_m}, {}^r x_{N_m}^r, n_{N_m}, \underline{s}_{N_m}, \bar{s}_{N_m}) \in (\mathbb{R}_{>0} \times \mathbb{R}^3 \times \mathbb{S}^2 \times \mathbb{R} \times \mathbb{R})^{N_m}$.

B. Dynamics

The objective of the ABS is to move the balancing masses in such a way that the in-plane components of the reaction force and torque at the interface point, which are measured by sensors, are ideally canceled. To understand how the inertial unbalances of the rotor affect those quantities, we apply Euler-Newton's law to the rotor and the ABS system (*i.e.*, the overall payload):

$$ \frac{dq}{dt} = f^e + f_O \tag{8} $$

$$ \frac{dh_O}{dt} = -v_O \times q + \tau_O^e + \tau_O \tag{9} $$

where

$$
\begin{aligned}
q &:= m_r {}^i v_G^i + \sum_{j=1}^{N_m} m_j {}^i v_j^i \\
&= m_p {}^i v_O^i + m_r R_r^i S({}^r\omega^i) {}^r x_{G_p}^r + R_r^i \sum_{j=1}^{N_m} m_j \dot{s}_j n_j \qquad (10) \\
h_O &:= m_r S(R_r^i {}^r x_G^r) {}^i v_O^i + R_r^i J_r \omega + \sum_{j=1}^{N_m} r_j \times m_j {}^i v_j^i \\
&= m_p S(R_r^i {}^r x_{G_p}^r) {}^i v_O^i + R_r^i J_r {}^r\omega^i \\
&+ R_r^i \sum_{j=1}^{N_m} m_j (S({}^r x_j^r + s_j n_j) S({}^r x_j^r + s_j n_j)^\top {}^r\omega^i + S({}^r x_j^r) n_j \dot{s}_j)) \qquad (11)
\end{aligned}
$$

are the translational and the angular momentum, respectively. The exogenous force and torque have been split in contributions associated with the interface reaction at O (f_O and τ_O) and in contributions associated with environmental effects (f^e and τ_O^e). Herein, $J_r \in \mathbb{R}^{3\times3}$ and $m_r \in \mathbb{R}_{>0}$ are the inertia matrix, with respect to O and expressed in $\mathcal{F}_r$, and the mass of the rotor, respectively, while $m_p := m_r + \sum_{j=1}^{N_m} m_j$ is the total mass of the payload and ${}^r x_{G_p}^r := \frac{1}{m_p}(m_r {}^r x_G^r + \sum_{j=1}^{N_m} m_j ({}^r x_j^r + s_j n_j))$ is the location of the center of mass of the payload.

Before proceeding, the following assumptions are considered to simplify the dynamical model in (8)-(9) to carry out the control design of the ABS controller.

Assumption 1 *Given any constant desired attitude $R_d \in \mathrm{SO}(3)$, the attitude control system of the spacecraft keeps the spacecraft attitude R_b^i close to the desired one R_d, so that one can consider $R_b^i(t) \equiv R_d \ \forall t \geq 0$ when designing the ABS controller.*

Remark 1 The above assumption is reasonable as the magnitude of the unbalance force and torque are dependent on the rotor speed, as shown next, and in a plausible scenario the rotor will be spun up slowly to avoid the risks associated with large unbalances. Moreover, based on the results of [10], a properly designed and tuned attitude control system for the spacecraft base can keep the attitude stable in the presence of a rotating unbalanced device, with guaranteed convergence to the desired attitude for vanishing unbalances. Small mismatches with respect to the perfect stabilization condition embedded in Assumption 1 will be treated as disturbance terms acting on the nominal model. ⌟

Assumption 2 *The exogenous force and torque acting on the payload are given by*

$$
{}^i f^e := {}^i f^g + \Delta f^e \qquad (12)
$$

$$
{}^i \tau_O^e := R_r^i {}^r x_{G_p}^r \times {}^i f^g + \Delta \tau_O^e, \qquad (13)
$$

where ${}^i f^g := -\mu^{\oplus} m_p \frac{{}^i x^i_{G_p}}{\|{}^i x^i_{G_p}\|^3}$, *with* $\mu^{\oplus}$ *being the product of gravitational constant and the mass of the earth, while* $\Delta f^e \in \mathbb{R}^3$ *and* $\Delta\tau^e_O \in \mathbb{R}^3$ *represent unmodelled disturbances.*

Remark 2 Assumption 2 implies that the main source of the exogenous force and torque is due to the gravity field, derived using a point mass model of the payload. Unmodelled (second order) effects associated with the actual mass distribution of the system and other environmental perturbations are included in the terms Δf^e and $\Delta\tau^e$, which will be dealt with a robust control design. It is worth underlying that the approximation introduced through Assumption 2 essentially splits the overall motion of the spacecraft into the orbital motion of a point having the total mass of the system and a superimposed relative motion, as if the spacecraft is floating without gravity. As shown next, Assumption 1 and Assumption 2 allow for the development of a decoupled control architecture in which the ABS control design can be carried out independently of the spacecraft attitude control, the latter being considered in [10]. ⌟

Let us focus on the translational dynamics first. By substituting (10) into the left-hand side of (8), we have:

$$\begin{aligned}\frac{dq}{dt} = m_p\, {}^i\dot{v}^i_O + R^i_r \sum_{j=1}^{N_m} m_j \left(S({}^r\omega^i)\dot{s}_j n_j + \ddot{s}_j n_j\right) \\ + \dot{R}^i_r \left(m_p S({}^r\omega^i)\, {}^r x^r_{G_p}) + \sum_{j=1}^{N_m} m_j (S({}^r\omega^i)({}^r x^r_j + s_j n_j) + \dot{s}_j n_j) \right) \\ + R^i_r \left(m_p S({}^r\dot{\omega}^i)\, {}^r x^r_{G_p}) + \sum_{j=1}^{N_m} m_j (S({}^r\dot{\omega}^i)({}^r x^r_j + s_j n_j) + \dot{s}_j n_j) \right). \quad (14)\end{aligned}$$

Based on Assumption 1, one also has ${}^b\omega^i(t) = {}^b\dot{\omega}^i(t) \equiv 0\ \forall t \geq 0$. Since the payload is rotating at constant rate, $\dot{\Omega}(t) \equiv 0\, \forall t \geq 0$, it follows that the angular acceleration of the payload is identically zero as well, *i.e.*, ${}^r\dot{\omega}^i = \dot{\omega} + \dot{\Omega} e_3 \equiv 0$. Further assuming that the orbital acceleration times the mass of the payload is mostly balanced by the gravity force, *i.e.*, $m_p\, {}^i\dot{v}^i_O \dot{\approx} f^g$ (we embed the mismatch into the disturbance term Δf^e), using (10), (14) and (12) the interface force can be approximated by the following expression:

$$\begin{aligned}{}^i f_O = R^i_r S(\Omega e_3) \left(m_r S(\Omega e_3)\, {}^r x^r_{G_p}) + \sum_{j=1}^{N_m} m_j \dot{s}_j n_j + S(\Omega e_3)({}^r x^r_j + s_j n_j) \right) \\ + R^i_r \left(\sum_{j=1}^{N_m} m_j \ddot{s}_j n_j + S(\Omega e_3)\dot{s}_j n_j \right) + \Delta f^e. \quad (15)\end{aligned}$$

We can now proceed similarly for the angular dynamics (9). To this end, consider the following equalities:

$$
\begin{aligned}
{}^i\dot{v}^i_O \times q &= S({}^iv^i_O)m_p{}^iv^i_O + S({}^iv^i_O)(m_rR^i_rS({}^r\omega^i){}^rx^r_{G_p} + R^i_r\sum_{j=1}^{N_m} m_j\dot{s}_jn_j) \\
&= -S(m_pR^i_rS({}^r\omega^i){}^rx^r_{G_p} + R^i_r\sum_{j=1}^{N_m} m_j\dot{s}_jn_j){}^iv^i_O \\
&= -S(m_pR^i_rS({}^r\omega^i){}^rx^r_{G_p} + R^i_r\sum_{j=1}^{N_m} m_j\dot{s}_jn_j){}^iv^i_O, \qquad (16) \\
\frac{d}{dt}m_pS(R^{i\,r}_rx^r_{G_p})v_O &= m_pS(R^i_rS({}^r\omega^i){}^rx^r_{G_p} + R^{i\,r}_r\dot{x}^r_{G_p}){}^iv^i_O + m_pS(R^{i\,r}_rx^r_{G_p}){}^i\dot{v}^i_O \\
&= S(m_pR^i_rS({}^r\omega^i){}^rx^r_{G_p} + R^i_r\sum_{j=1}^{N_m} m_j\dot{s}_jn_j){}^iv^i_O + S(R^{i\,r}_rx^r_{G_p})f^g, \qquad (17)
\end{aligned}
$$

where we exploited that $S(v_O)m_pv_O = m_pv_O \times v_O = 0$ and then used the approximation $m_p\dot{v}_O \approx f^g$, which was already introduced when deriving the approximated translational dynamics. Using (16) and (17), one obtains ${}^iv^i_O \times q + \frac{d}{dt}m_pS(R^{i\,r}_rx^r_{G_p}) = S(R^{i\,r}_rx^r_{G_p})f^g$. Then, substituting (13) into (9), and performing some computations, we obtain the following expression for the approximated interface torque:

$$
\begin{aligned}
{}^i\tau_O = R^i_rS(\Omega e_3)\Bigg(&J_r\omega + \sum_{j=1}^{N_m} m_jS({}^rx^r_j + s_jn_j)S^\top({}^rx^r_j + s_jn_j)\Omega e_3 + \\
&+ \sum_{j=1}^{N_m} m_jS({}^rx^r_j)n_j\dot{s}_j\Bigg) + R^i_r\Bigg(\sum_{j=1}^{N_m} m_j\Big(S(n_j)S^\top({}^rx^r_j + s_jn_j) + \\
&+S({}^rx^r_j + s_jn_j)S^\top(n_j)\Big)\Omega e_3\dot{s}_j + \sum_{j=1}^{N_m} m_jS({}^rx^r_j)n_j\ddot{s}_j\Bigg) + \Delta\tau^e_O \qquad (18)
\end{aligned}
$$

where we considered the same approximations adopted for the translational dynamics stemming from Assumption 1. As the ABS setup described in the Introduction makes use of sensors that measure the interface force and torque in frame $\mathcal{F}_a$, it is necessary to express (15) and (18) in such a frame. To this end, multiplying both sides of (15)-(18) by $R^{b\top}$, the in-plane components of f_O and τ_O in $\mathcal{F}_a$ can be compactly written as follows:

$$
\begin{bmatrix} {}^af_{O_1} \\ {}^af_{O_2} \\ {}^a\tau_{O_1} \\ {}^a\tau_{O_2} \end{bmatrix} = \underbrace{\begin{bmatrix} c(\theta(t)) & -s(\theta(t)) & 0 & 0 \\ s(\theta(t)) & c(\theta(t)) & 0 & 0 \\ 0 & 0 & c(\theta(t)) & -s(\theta(t)) \\ & & 0 & s(\theta(t)) \quad c(\theta(t)) \end{bmatrix}}_{Z(t)} \begin{bmatrix} {}^rf_{O_1} \\ {}^rf_{O_2} \\ {}^r\tau_{O_1} \\ {}^r\tau_{O_2} \end{bmatrix}, \qquad (19)
$$

where $c(\cdot)$, $s(\cdot)$ is a shorthand notation for $\cos(\cdot)$, $\sin(\cdot)$, respectively, and the expressions of f_O^r, τ_O^r are reported in equations (20) through (23).

Given the approximations introduced to derive the mathematical model in (19), the dynamics of the rotating device under an attitude controlled base has been reduced to the one of a ground fixed system, thereby effectively enabling a decoupled design for the attitude controller of the base and the control system of the ABS and giving the possibility of testing the ABS on ground by building a suitable breadboard, as discussed in Section V.A.

$$
{}^r f_{O_1} = -\Omega^2 \left(m_r {}^r x_{G,1}^r + \sum_{j=1}^{N_m} m_j (\bar{x}_j + s_j e_1^\top n_j) \right) + 2\Omega \sum_{j=1}^{N_m} m_j e_2^\top n_j \dot{s}_j + \sum_{j=1}^{N_m} m_j e_1^\top n_j \ddot{s}_j + \Delta f_1^e \tag{20}
$$

$$
{}^r f_{O_2} = -\Omega^2 \left(m_r {}^r x_{G,2}^r + \sum_{j=1}^{N_m} m_j (\bar{y}_j + s_j e_2^\top n_j) \right) - 2\Omega \sum_{j=1}^{N_m} m_j e_1^\top n_j \dot{s}_j + \sum_{j=1}^{N_m} m_j e_2^\top n_j \ddot{s}_j + \Delta f_2^e \tag{21}
$$

$$
\begin{aligned}
{}^r \tau_{O_1} = -\Omega^2 \Bigg(J_{r,23} - \sum_{j=1}^{N_m} m_j (\bar{y}_j + s_j e_2^\top n_j)(\bar{z}_j + s_j e_3^\top n_j) \Bigg) + \sum_{j=1}^{N_m} m_j \begin{bmatrix} 0 & -\bar{z}_j & \bar{y}_j \end{bmatrix} n_j \ddot{s}_j + \Omega \sum_{j=1}^{N_m} m_j \Bigg(\Bigg[\begin{bmatrix} -\bar{z}_j & 0 & \bar{x}_j \end{bmatrix} n_j + \\
+ e_1^\top S(n_j) \begin{bmatrix} -\bar{y}_j - s_j e_2^\top n_j & \bar{x}_j + s_j e_1^\top n_j & 0 \end{bmatrix}^\top + \begin{bmatrix} 0 & -\bar{z}_j - s_j e_3^\top n_j & \bar{y}_j + s_j e_2^\top n_j \end{bmatrix} S^\top (n_j) e_3 \Bigg) \dot{s}_j + \Delta \tau_{O_1}^e
\end{aligned} \tag{22}
$$

$$
\begin{aligned}
{}^r \tau_{O_2} = \Omega^2 \Bigg(J_{r,13} - \sum_{j=1}^{N_m} m_j (\bar{x}_j + s_j e_1^\top n_j)(\bar{z}_j + s_j e_3^\top n_j) \Bigg) + \sum_{j=1}^{N_m} m_j \begin{bmatrix} \bar{z}_j & 0 & -\bar{x}_j \end{bmatrix} n_j \ddot{s}_j + \Omega \sum_{j=1}^{N_m} m_j \Bigg(\Bigg[\begin{bmatrix} 0 & -\bar{z}_j & \bar{y}_j \end{bmatrix} n_j + \\
+ e_2^\top S(n_j) \begin{bmatrix} -\bar{y}_j - s_j e_2^\top n_j & \bar{x}_j + s_j e_1^\top n_j & 0 \end{bmatrix}^\top + \begin{bmatrix} \bar{z}_j + s_j e_3^\top n_j & 0 & -\bar{x}_j - s_j e_1^\top n_j \end{bmatrix} S^\top (n_j) e_3 \Bigg) \dot{s}_j + \Delta \tau_{O_1}^e .
\end{aligned} \tag{23}
$$

C. Control problem formulation

To describe the balancing control problem based on the dynamic model derived in the previous section, we first characterize the necessary control authority of the ABS to achieve a balanced configuration. Without loss of generality,

assume that the rotor and the ABS unbalances for $s_j = 0$ can be split in nominal and perturbation terms as follows:

$$m_r {}^r x^r_{G,1} + \sum_{j=1}^{N_m} m_j \bar{x}_j = \bar{S}_1 + \Delta S_1 = \Delta S_1 \tag{24}$$

$$J_{r,13} - \sum_{j=1}^{N_m} m_j \bar{x}_j \bar{z}_j = \bar{J}_{13} + \Delta J_{13} = \Delta J_{13} \tag{25}$$

$$m_r {}^r x^r_{G,2} + \sum_{j=1}^{N_m} m_j \bar{y}_j = \bar{S}_2 + \Delta S_2 = \Delta S_2 \tag{26}$$

$$J_{r,23} - \sum_{j=1}^{N_m} m_j \bar{y}_j \bar{z}_j = \bar{J}_{23} + \Delta J_{23} = \Delta J_{23} \tag{27}$$

where, given $i = 2, 3$, $\bar{S}_i$ and ΔS_i denote the static moment and the corresponding perturbation and similarly $\bar{J}_{i3}$ and ΔJ_{i3} denote the nominal inertia moment and the corresponding perturbation. The idea behind the decomposition in (24)-(27) is that the rotor and the ABS are designed to be self-balanced ($\bar{S}_1 = \bar{S}_2 = 0$, $\bar{J}_{13} = \bar{J}_{23} = 0$) but that there will be unavoidably residual unbalances in practice. Of note, for constant unbalances, balanced equilibrium conditions ($\dot{s}_j = \ddot{s}_j = {}^r f_{O_1}{}^r = {}^r f_{O_2} = {}^r \tau_{O_1} = {}^r \tau_{O_2} = 0$) can be obtained provided that the ABS satisfies the following assumption.

Assumption 3 *Given positive scalars* $\bar{\Delta}_i \in \mathbb{R}_{>0}$, $j = 1, \ldots, 4$, *for any* $[\ {}^{\Delta S_1}\ {}^{\Delta S_2}\ {}^{\Delta J_{13}}\ {}^{\Delta J_{23}}\ ]^\top \in \Omega_\Delta := \left\{\Delta \in \mathbb{R}^4 : |\Delta_i| \leq \bar{\Delta}_i,\right.$ $\left. i = 1, \ldots, 4\right\}$, *the ABS* $(m_j, {}^r x^r_j, n_j, \underline{s}_j, \bar{s}_j)$, $j = 1, \ldots, N_m$, *is such that the system of algebraic equation*

$$\sum_{j=1}^{N_m} m_j e_1^\top n_j s_j = -\Delta S_1 \tag{28}$$

$$\sum_{j=1}^{N_m} m_j e_2^\top n_j s_j = -\Delta S_2 \tag{29}$$

$$\sum_{j=1}^{N_m} m_j \left((e_2^\top n_j)(e_3^\top n_j) s_j^2 \bar{y}_j (e_3^\top n_j) + \bar{z}_j (e_2^\top n_j) s_j \right) = \Delta J_{23} \tag{30}$$

$$\sum_{j=1}^{N_m} m_j \left((e_1^\top n_j)(e_3^\top n_j) s_j^2 \bar{x}_j (e_3^\top n_j) + \bar{z}_j (e_1^\top n_j) s_j \right) = \Delta J_{13} \tag{31}$$

admits at least one feasible solution, i.e.*, there exist positions of the balancing masses solving* (28)-(31) *and such that* $s_j \in [\underline{s}_j, \bar{s}_j]\ \forall j = 1, \ldots, N_m$.

Note that system (28)-(31) is obtained by substituting equations (24)-(27) in (20)-(23) and then by setting to zero the terms that multiply Ω^2. The above assumption is necessary to have a feasible control problem, as more formally defined at the end of this section. By defining $w := [\ {}^r f_{O_1}\ {}^r f_{O_2}\ {}^r \tau_{O_1}\ {}^r \tau_{O_2}\ ]^\top$ and by means of (24)-(27), equations (20)-(23) can be compactly written as:

$$w = \sum_{j=1}^{N_m} C^j_{abs} y^j_a + D_{abs} d \tag{32}$$

where $y_a^i = [\, s_j \;\; \dot{s}_j \;\; \ddot{s}_j \,]^\top$ and $d := [\, \Delta S_1 \;\; \Delta S_2 \;\; \Delta J_{13} \;\; \Delta J_{23} \,]^\top$ and the exogenous disturbances have been neglected for the purpose of deriving the nominal model for control. The exact expressions of C_{abs}^i and D_{abs} can be derived from (20)-(23) but they are omitted here for space reasons. The ABS system includes N_m position-controlled linear actuators to assign the motion of the balancing masses. Assuming a linear model for the closed-loop behavior of the actuators, we can compactly write the actuators dynamics as

$$\dot{x}_a = A_a x_a + B_a u, \qquad y_a = C_a x_a + D_a u, \tag{33}$$

where $x_a = [\, x_a^1 \;\cdots\; x_a^{N_m} \,]^\top \in \mathbb{R}^{N_m N_a}$ is a vector including all the states of the N_m actuators, $y_a = [\, y_a^i \;\cdots\; y_a^{N_m} \,]^\top \in \mathbb{R}^{3N_m}$ is a vector collecting the outputs defined in (32) and $u = [\, u_1 \;\cdots\; u_{N_m} \,] \in \mathbb{R}^{N_m}$ is the vector of control variables, *i.e.*, the desired positions of the ABS masses. Finally, $A_a = \text{blkdiag}(A_a^j)$, $B_a = \text{blkdiag}(B_a^j)$, $C_a = \text{blkdiag}(C_a^j)$ and $D_a = \text{blkdiag}(D_a^j)$ are block diagonal matrices formed from the quadruples $(A_a^j, B_a^j, C_a^j, D_a^j)$ characterizing the *j-th* actuator dynamics, which has order N_a. The in-plane torque and force in the spacecraft-base frame (equation (19)) are measured by load sensors, for which we again assume a linear behavior, given by:

$$\begin{aligned} \dot{x}_s &= A_s x_s + B_s Z(t) w \\ &= A_s x_s + B_s Z(t) \left(C_{abs} C_a x_a + C_{abs} D_a u + D_{abs} d \right) \end{aligned} \tag{34}$$

$$y_s = C_s x_s \tag{35}$$

where $C_{abs} = [\, C_{abs}^1 \;\cdots\; C_{abs}^{N_m} \,]$, $Z(t)$ is defined in (19) and $A_s = \text{blkdiag}(A_s^i)$, $B_s = \text{blkdiag}(B_s^i)$, $C_s = \text{blkdiag}(C_s^i)$ are block diagonal matrices formed from the triples (A_s^i, B_s^i, C_s^i) characterizing the *i-th* load sensor dynamics, which has order N_s. By defining $x = [\, x_a \;\; x_s \,]^\top$ and $y = y_s \in \mathbb{R}^4$, the overall system can be written in state-space form as follows:

$$\dot{x} = A(t)x + B_u(t)u + B_d(t)d \qquad y = \begin{bmatrix} 0 & C_s \end{bmatrix} x \tag{36}$$

where

$$\begin{aligned} A(t) &= \begin{bmatrix} A_a & 0 \\ B_s Z(t) C_{abs} C_a & A_s \end{bmatrix}, \quad B_u(t) = \begin{bmatrix} B_a \\ B_s Z(t) C_{abs} D_a \end{bmatrix}, \\ B_d(t) &= \begin{bmatrix} 0 \\ B_s Z(t) D_{abs} \end{bmatrix}. \end{aligned} \tag{37}$$

Remark 3 While the assumption of linearity in the behavior of both the actuators and sensors may not be true in practice, the approximation allows us to perform a preliminary verification of the control design in simulation. This is

also not an issue in practical implementations for the considered application, where the proposed control law can be applied after the actuators have reached their desired positions and the load cell sensors are so fast that their dynamics can be neglected, as it is done in our experiments reported in Section V.E. ⌟

By referring to system (36), the problem that we address in this work can be formulated as the design of an output feedback controller for u (desired positions of the ABS masses) such that the measured interface loads y are minimized for all inertial unbalances satisfying $|d_i| \leq \bar{\Delta}_i$, $i = 1, \ldots, 4$, where $\bar{\Delta}_i \in \mathbb{R}_{>0}$ are the minimum unbalances that the ABS should be able to compensate for according to Assumption 3.

IV. CONTROL LAW DESIGN

The model of the rotor and the ABS in equation (36) is represented by a Linear Time Periodic (LTP) system. In this section we will propose a control design exploiting piece-wise constant inputs to solve the rotor balancing problem by leveraging Harmonic Control (short, HC) theory. Firstly we briefly recall the main ideas behind HC and then we present the steps for the derivation of the control law according to the T-matrix HC algorithm, following the approaches in [17, 18].

A. Harmonic Transfer Function formulation

The steady-state response of a LTP system can be characterized by the Harmonic Transfer Function (HTF), which is an extension to periodic systems of the frequency response function of a time-invariant system. In order to compute the HTF we follow the approach described in [18, 19], which we briefly recall. By deriving Fourier expansions for $A(t)$, $B_u(t)$, $B_d(t)$, $C(t)$ and $D(t)$ (*e.g.*, $A(t) = \sum_{m=-\infty}^{m=+\infty} A_m \exp(jm\Omega t)$), it is possible to prove that the Exponentially Modulated Periodic (EMP) steady-state response of system (36) can be expressed as the infinite dimensional matrix equation with *constant* elements

$$s\mathcal{X} = (\mathcal{A} - \mathcal{N})\mathcal{X} + \mathcal{B}_u\mathcal{U} + \mathcal{B}_d\mathcal{D}, \qquad \mathcal{Y} = \mathcal{C}\mathcal{X} \tag{38}$$

where $\mathcal{X}, \mathcal{U}, \mathcal{D}$ and $\mathcal{Y}$ are doubly infinite vectors formed with the harmonics of x, u, d, and y respectively, organized as $\mathcal{X}^\top = \begin{bmatrix} \cdots & x_{-2}^\top & x_{-1}^\top & x_0^\top & x_1^\top & x_2^\top & \cdots \end{bmatrix}$ and similarly for $\mathcal{U}$ and $\mathcal{Y}$. $\mathcal{A}$, $\mathcal{B}$ and $\mathcal{C}$ are doubly infinite Toeplitz matrices formed with the harmonics of $A(\cdot)$, $B(\cdot)$ and $C(\cdot)$, and $\mathcal{N}$ is a block diagonal complex-valued matrix given by $\mathcal{N} = \text{blkdiag}\{jm\Omega I\}$ where I is the identity matrix the size of which is equal to the number of states (see [18] for more details). From equation (38), one can define the HTF operator

$$\mathcal{G}_u(s) = \mathcal{C}[s\mathcal{I} - (\mathcal{A} - \mathcal{N})]^{-1}\mathcal{B}_u, \tag{39}$$

which relates the input harmonics and the output harmonics (contained in the infinite vectors $\mathcal{U}$ and $\mathcal{Y}$ respectively), and the disturbance HTF operator

$$\mathcal{G}_d(s) = \mathcal{C}[s\mathcal{I} - (\mathcal{A} - \mathcal{N})]^{-1}\mathcal{B}_d, \tag{40}$$

where $\mathcal{I}$ is an infinite dimensional identity matrix. It can be noticed that the rotor will be subject to a proper, steady-state harmonic control input whenever the control vector u is *constant* (the same consideration holds for the disturbance d). This implies that we only have to study the response of the periodic model to a EMP input with $s = 0$, *i.e.*, we only have to compute the input/output operators $\mathcal{G}_u(0)$ and $\mathcal{G}_d(0)$. Given a constant input $u(t) = u_0$, the vector $\mathcal{U}$ corresponding to $u(t) = u_0$ is given by

$$\mathcal{U}^T = \begin{bmatrix} \cdots & 0 & 0 & u_0^T & 0 & 0 & \cdots \end{bmatrix} \tag{41}$$

and the steady-state response $\mathcal{Y}$ of the periodic system without the disturbance is given by

$$\mathcal{Y} = \mathcal{G}_u(0)\mathcal{U} \tag{42}$$

which can be equivalently written as

$$\begin{bmatrix} \vdots \\ y_{-1} \\ y_0 \\ y_1 \\ \vdots \end{bmatrix} = \begin{bmatrix} \ddots & \vdots & \vdots & \vdots & \\ \cdots & G^{\,u}_{-1,-1} & G^{\,u}_{-1,0} & G^{\,u}_{-1,1} & \cdots \\ \cdots & G^{\,u}_{0,-1} & G^{\,u}_{0,0} & G^{\,u}_{0,1} & \cdots \\ \cdots & G^{\,u}_{1,-1} & G^{\,u}_{1,0} & G^{\,u}_{1,1} & \cdots \\ & \vdots & \vdots & \vdots & \ddots \end{bmatrix} \begin{bmatrix} \vdots \\ 0 \\ u_0 \\ 0 \\ \vdots \end{bmatrix} \tag{43}$$

Focusing on the N-harmonics, from equation (43) we have that

$$\begin{bmatrix} y_{-1} \\ y_1 \end{bmatrix} = \begin{bmatrix} G^{\,u}_{-1,0} \\ G^{\,u}_{1,0} \end{bmatrix} u_0. \tag{44}$$

Converting the harmonics of the output from exponential to trigonometric form, the following expression is obtained:

$$\begin{bmatrix} y_{1c} \\ y_{1s} \end{bmatrix} = Tu_0, \tag{45}$$

where

$$T := 2 \begin{bmatrix} \text{Real}[G^{u}_{1,0}] \\ \text{Imag}[G^{u}_{1,0}] \end{bmatrix} \in \mathbb{R}^{2n_y \times n_u} \tag{46}$$

is known in the literature as the T-matrix.

B. LQ-based HC algorithm

Let us assume that the update of the control input $u(t)$ is at specific times $t_k = k\Delta t$, where Δt is the time interval between consecutive updates, during which the plant output is assumed to reach a steady level, and where $k \in \mathbb{Z}_{\geq 0}$ is the discrete-time index. Based on the results of the previous section, the steady-state response of the system (36) to both inputs and disturbances can be expressed by the following discrete time mathematical model:

$$y_1(k) = Tu(k) + Wd, \tag{47}$$

where $y_1 \in \mathbb{R}^{2n_y}$ is the vector of the first harmonics of measured outputs, namely,

$$y_1(k) = \begin{bmatrix} y_{1c}(k) \\ y_{1s}(k) \end{bmatrix} = \begin{bmatrix} \frac{1}{\pi} \int_{k\pi}^{(k+1)\pi} y(\psi) \cos(N\psi)\ d\psi \\ \\ \frac{1}{\pi} \int_{k\pi}^{(k+1)\pi} y(\psi) \sin(N\psi)\ d\psi \end{bmatrix} \quad \text{with } \psi = \Omega t\ , \tag{48}$$

u is the vector of the desired positions of the ABS masses in the rotating frame and d is the vector of the inertial unbalances defined below equation (32). The T matrix was already defined in (46) while $W \in 2n_y \times n_d$ is a constant matrix defined in similar fashion as

$$W = 2 \begin{bmatrix} \text{Real}[G^{d}_{1,0}] \\ \text{Imag}[G^{d}_{1,0}] \end{bmatrix}. \tag{49}$$

For system (47), HC is a viable approach for the design of a feedback controller aiming at the minimization of the measured interface loads. The conventional HC control law is derived by minimizing at each discrete-time step k the cost function

$$J(k) = y_1(k)^\top Q y_1(k) + u(k)^\top R u(k) \tag{50}$$

where $Q = Q^\top \geq 0$, $R = R^\top > 0$. Differentiating equation (50) with respect to $u(k)$ yields the T-matrix control law

$$u(k+1) = KTu(k) - Ky_1(k) \tag{51}$$

where $K = (T^\top QT + R)^{-1}T^\top Q$ is a gain matrix.

C. Convergence analysis of the HC algorithm

At each time t_k, the vibrations/effects induced by the unbalances can be evaluated as

$$Wd = y_1(k) - Tu(k). \tag{52}$$

Therefore, by substituting (52) into (47) evaluated at $k+1$ one obtains

$$\begin{aligned} y_1(k+1) &= Tu(k+1) + y_1(k) - Tu(k) \\ &= TKTu(k) - TKy_1(k) + y_1(k) - Tu(k) \\ &= (I - TK)y_1(k) + T(KT - I)u(k). \end{aligned} \tag{53}$$

As discussed in [17], with initial conditions $y_1(0)$ and $u(0)$, the system dynamics (53) is equivalent to

$$\begin{bmatrix} y_1(k+1) \\ u(k+1) \end{bmatrix} = A_T \begin{bmatrix} y_1(0) \\ u(0) \end{bmatrix} \tag{54}$$

$\forall k \geq 0$, where

$$A_T := \begin{bmatrix} I - TK & T(KT - I) \\ -K & KT \end{bmatrix}. \tag{55}$$

As a result, the optimal values of $y_1(k)$ and $u(k)$ are attained after the first update.

Remark 4 This result holds true under the assumption that T-matrix is known. If the T-matrix is uncertain, HC could result in degraded performance and possible instability (see the next Section for the robustness analysis with respect to an uncertain T). Moreover, the one-step convergence property decays. ⌟

Based on equation (54), the steady output can be written by means of the relation

$$y_{opt} := y_1(k) = K_{LQ}\left(y_1(0) - Tu(0)\right) = K_{LQ}Wd, \tag{56}$$

where

$$K_{LQ} = Q^{-1}\left(Q^{-1} + TR^{-1}T^T\right)^{-1} \tag{57}$$

is a gain matrix which allows to estimate the "distance" from the complete reduction of the disturbance d. Furthermore, following the steps described in [17], an upper bound of $\|y_1(k)\|$ is obtained as

$$\|y_1(k)\| \leq \frac{\sigma_{max}(R)}{\sigma_{min}(Q)\sigma_i(TT^T)}\|Wd\|, \tag{58}$$

where $i = \min(2n_y, 2n_u)$.

D. Robustness analysis of the HC control algorithm

The analysis of the previous section is interesting because it shows that the LQ-based HC ensures a bounded output for any bounded disturbance with a tunable upper bound, thereby granting robustness with respect to exogenous perturbations, as also confirmed by previous studies in [9, 18, 20, 21]. At the same time, the implementation of HC requires knowledge of the T-matrix: as noted in Remark 4, an erroneous model of the system results in a wrong T which can in turn degrade performance and possibly lead to instability. Given the approximations introduced in deriving the model for control, it worth understanding the robustness of the proposed algorithm with respect to model variations. To this aim, if an estimate $\hat{T}$ of T is given as

$$\hat{T} = T + \Delta T, \tag{59}$$

then the control law defined in equation (51) becomes

$$u(k+1) = -\hat{T}\hat{K}u(k) + \hat{K}y_1(k), \tag{60}$$

where

$$\hat{K} = -(\hat{T}^T Q\hat{T} + R)^{-1}(\hat{T}^T Q). \tag{61}$$

As discussed in [20] the stability of the HC algorithm requires that

$$\rho_s(\hat{K}\Delta T) < 1, \tag{62}$$

where $\rho_s(\cdot)$ is the spectral radius. An upper bound on the spectral radius of $\hat{K}\Delta T$ can be derived by using (61) to obtain:

$$\begin{aligned}\rho_s(\hat{K}\Delta T) &= \rho_s((\hat{T}^T Q\hat{T} + R)^{-1}\hat{T}^T Q\Delta T) \\ &\leq \frac{(\sigma_{max}(T) + \sigma_{max}(\Delta T))\,\sigma_{max}(Q)\sigma_{max}(\Delta T)}{\sigma_{min}(R)}.\end{aligned} \tag{63}$$

In [20] it has been shown that if

$$\sigma_{max}(\Delta T) < -\frac{\sigma_{max}(T)}{2} + \frac{1}{2}\sqrt{\sigma_{max}(T)^2 + 4\frac{\sigma_{min}(R)}{\sigma_{max}(Q)}}\,, \tag{64}$$

then $\rho_s(\hat{K}\Delta T) < 1$.

Remark 5 As noted in [17], there is evidence from equations (58) and (64) of the presence of a trade-off between performance and robustness properties of the closed-loop system. If the ratio $\rho := \frac{\sigma_{min}(R)}{\sigma_{max}(Q)}$ is large, *i.e.*, tuning aims at minimum control effort (see equation (50)), then, according to inequality (64), the control law achieves a high degree of robustness against parametric uncertainties. However, inequality (58) suggests that poor disturbance attenuation performance must be expected for large values of ρ. ⌟

Remark 6 The validity of the previous method is predicated on the control input being updated slowly enough that transient dynamics do not affect the steady response measurements. Note that, if the transient dynamics is not allowed to dissipate, the overall closed-loop response at the sample times will contain a non-zero spurious component corresponding to the zero-input response of the states, resulting in erroneous control amplitude and phase estimates for the next iteration. This is in fact equivalent to introducing model uncertainty in the estimate of the T-matrix. For the space application considered in this work, the control law update time can be much larger with respect to the decay time of the transient dynamics (given that the balancing masses can be moved slowly), avoiding the excitation of the system transient behavior.. ⌟

V. Simulation and experimental results

By carefully inspecting equations (20)-(23), one sees that the balancing problem can be decoupled in two sub-problems, one for the xz plane and one for the yz plane, provided that the ABS is made of a suitable set of strokes directed along the coordinate axes. Based on this idea, a breadboard representative of a single-plane ABS has been designed and built to test the proposed control design.

A. ABS breadboard design and modeling

The breadboard (see Figure 3 and Figure 10) has been designed with an ABS made of three movable counter-masses lying in the xz plane of the rotor frame: a central mass, which can be moved along the x-axis ($n_1 = e_1$), and two side masses, which can be moved along the z-axis ($n_{2,3} = e_3$). While two masses would have been enough to balance the system, three masses give more flexibility and allow to easily obtain a self-balanced ABS. The main components of the breadboard are:

- the rotor structure, with the possibility of applying a known unbalance (static and dynamic) through the placement of four masses at the corners;

- three guides, each endowed with a linear actuator, to move the counter-mass;
- three load cell sensors in an equilateral triangle configuration forming a dynamometer;
- the stator structure;
- the rotary actuator, composed of motor, gearbox, and a differential digital encoder to rotate the rotor shaft;
- the slip ring, to guarantee the electrical connection between rotor and stator;
- the power supply, acquisition system, conditioners, and controllers.

The ABS configuration has been designed to be self-balanced, *i.e.*, when the counter masses are in their zero positions ($s_j = 0$) no unbalance is added to the system (see again equations (24)-(27)). The dynamometer allows the measurement of the interface force along the $x-$axis and the torque about the y-axis. The nominal angular rate of the rotor is $\Omega = 7.8$ rpm.

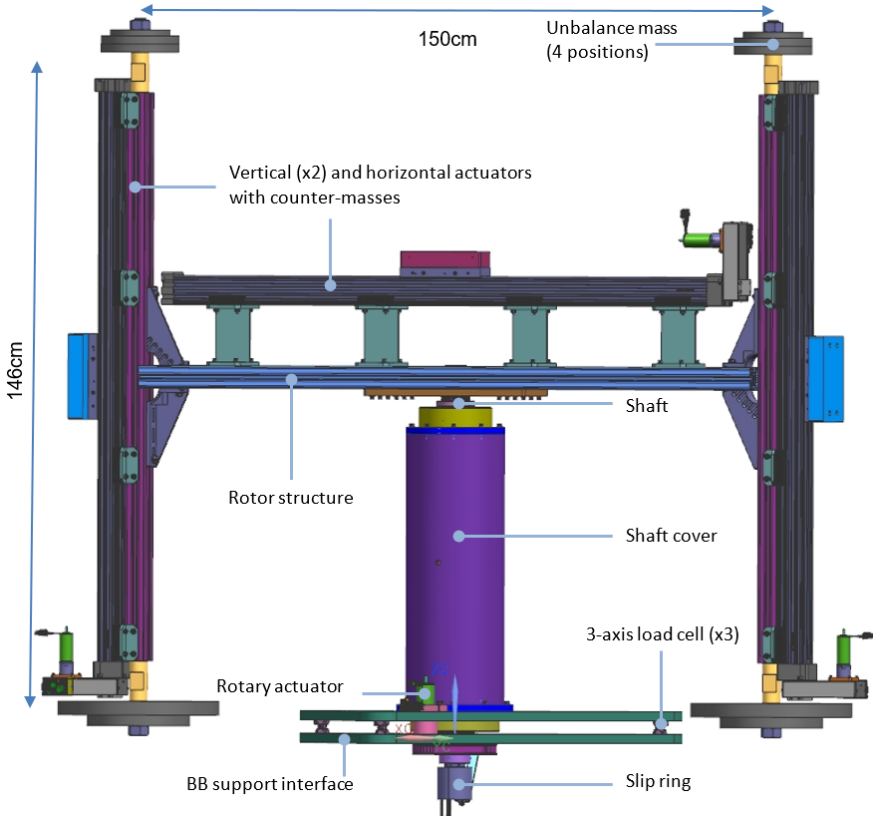

Figure 3 Multibody model of the breadboard.

For the considered setup, the reaction force ${}^r f_{O_1}$ (20) and torque ${}^r \tau_{O_2}$ (23) reduce to the following expressions:

$$
\begin{aligned}
{}^r f_{O_1} =& -\Omega^2 \left(\Delta S_1 + m_1 s_1\right) + m_1 \ddot{s}_1 - f_1^e && (65)\\
{}^r \tau_{O_2} =& \Omega^2 \left(\Delta J^{r,13} - m_1 \bar{z}_1 s_1 - m_2 \bar{x}_2 s_2 - m_3 \bar{x}_3 s_3\right) \\
&+ \sum_{j=1}^{3} m_j \left[\, \bar{z}_j \;\; 0 \;\; -\bar{x}_j \,\right] n_i \ddot{s}_j - \tau_{O_1}^e && (66)
\end{aligned}
$$

where $\Delta S_1 = \sum_{j=1}^{4} m_j^s \bar{x}_j^s$ and $\Delta J_{13}^r = \sum_{j=1}^{4} -m_j^s \bar{x}_j^s \bar{z}_j^s$. Herein $m_j^s \in \mathbb{R}_{>0}$ is the *j-th* unbalance mass and $x_j^s \in \mathbb{R}$ and $z_j^s \in \mathbb{R}$ represent the *j-th* unbalance mass and its coordinates in the xz plane, respectively. The exogenous force component f_1^e is associated with disturbances acting on the platform, such as, *e.g.*, friction between the rotor and the stator, small inclination of the structure with respect to the gravity direction, residual static unbalance in the structure, *etc.*. Instead, the exogenous torque mainly comprises the torque associated with gravity, *i.e.*,

$$
\tau_{O_1}^e \approx \sum_{j=1}^{4} m_j^s g x_j + m_r g^r x_G^r + m_1 g s_1, \tag{67}
$$

and the torque associated with an unavoidable residual unbalance in the structure.

Remark 7 While the gravity-induced torque (67) could be considered as a disturbance to be balanced by the harmonic controller (by including the term $m_1 g$ in matrix C_{abs}^1 in equation (32)), it was decided to remove it from the measured signal before applying the HC algorithm to better replicate on-orbit operations. ⌟

At this point, the dynamic model of the breadboard can be written in the same form as (36). Specifically, the matrices in equation (32), entering the dynamics through (37), are given by:

$$
C_{abs}^1 = m_1 \begin{bmatrix} -\Omega^2 & 0 & 1 \\ -\Omega^2 \bar{z}_1 & 0 & \bar{z}_1 \end{bmatrix}, \quad C_{abs}^2 = -m_2 \begin{bmatrix} 0 & 0 & 1 \\ \Omega^2 \bar{x}_2 & 0 & \bar{x}_2 \end{bmatrix}, \tag{68}
$$

$$
C_{abs}^2 = -m_3 \begin{bmatrix} 0 & 0 & 0 \\ \Omega^2 \bar{x}_3 & 0 & \bar{x}_3 \end{bmatrix}, \quad D_{abs} := \begin{bmatrix} -\Omega^2 & 0 \\ 0 & \Omega^2 \end{bmatrix}. \tag{69}
$$

For simplicity, we consider critically-damped second order systems for both the actuators and the sensors dynamics with unit DC-gain (which fully define matrices $A_a, B_a, C_a, D_a, A_s, B_s, C_s$). Matrix $A(t)$ defined as in (37), can be expanded in a complex Fourier series $A(t) = \sum_{m=-\infty}^{\infty} A_m e^{jm\Omega t}$: since $Z(t) = \begin{bmatrix} \cos(\theta(t)) & 0 \\ 0 & \cos(\theta(t)) \end{bmatrix}$ for the considered case, only the terms A_0, A_1 and A_{-1} are different from the null matrix. Expanding in the same fashion $B_u(t)$ and $C(t)$,

we consider the following finite-dimensional Toeplitz matrices

$$\mathcal{A} = \begin{bmatrix} A_0 & A_{-1} & 0 \\ A_1 & A_0 & A_{-1} \\ 0 & A_1 & A_0 \end{bmatrix} \qquad \mathcal{B}_u = \begin{bmatrix} B_{u_0} & 0 & 0 \\ 0 & B_{u_0} & 0 \\ 0 & 0 & B_{u_0} \end{bmatrix}$$
$$\mathcal{B}_d = \begin{bmatrix} B_{d_0} & B_{d_{-1}} & 0 \\ B_{d_1} & B_{d_0} & B_{d_{-1}} \\ 0 & B_{d_1} & B_{d_0} \end{bmatrix} \qquad \mathcal{C} = \begin{bmatrix} C_0 & 0 & 0 \\ 0 & C_0 & 0 \\ 0 & 0 & C_0 \end{bmatrix} \tag{70}$$

to compute the T-matrix as given by equation (46). The choice of the number of block rows used to approximate the infinite dimensional matrices in (39)-(40) will affect the numerical accuracy of the results (see [22] for an analysis of the effect of such a truncation in the study of frequency response operators). We found that using 3×3 block-matrices as in (70) was sufficient for our purposes.

B. ABS sizing and balancing capabilities

The proposed ABS is well-defined in the sense of Assumption 3 since the system

$$\begin{bmatrix} m_1 & 0 & 0 \\ m_1\bar{z}_1 & m_2\bar{x}_2 & m_3\bar{x}_3 \end{bmatrix} \begin{bmatrix} s_1 \\ s_2 \\ s_3 \end{bmatrix} = \begin{bmatrix} -\Delta S_1 \\ \Delta J_{13} \end{bmatrix}, \tag{71}$$

derived from equations (65)-(66), admits ∞^1 solutions provided that $\bar{x}_2$ and $\bar{x}_3$ are different from zero, *i.e.*, the system is overactuated. Of course, due to the finite length of the strokes ($\bar{s}_j = -\underline{s}_j = 0.5\,\text{m}$), the maximum static and dynamic unbalances which can be compensated are bounded. The balancing masses and their locations have been selected to counteract all the unbalances in the set $\Omega_\Delta := \left\{\Delta S_1,\ \Delta J_{13} \in \mathbb{R}^2 : |\Delta S_1| \leq \overline{\Delta S}_1,\ |\Delta J_{13}| \leq \overline{\Delta J}_{13}\right\}$, where $\overline{\Delta S}_1 = 2.2\,\text{kgm}$ and $\overline{\Delta J}_{13} = 4.5\,\text{kgm}^2$. The resulting ABS is characterized by the following parameters: $\bar{z}_1 = 0.98\,\text{m}$, $\bar{z}_2 = \bar{z}_3 = 0.72\,\text{m}$ $\bar{x}_2 = -\bar{x}_3 = 0.87\,\text{m}$, $m_1 = 4.6\,\text{kg}$ and $m_2 = m_3 = 8.1\,\text{kg}$. The balancing capabilities of the proposed sizing can be evaluated from (71) by computing the range of the map

$$(s_1, s_2, s_3) \mapsto \begin{bmatrix} m_1 & 0 & 0 \\ m_1\bar{z}_1 & m_2\bar{x}_2 & -m_3\bar{x}_2 \end{bmatrix} \begin{bmatrix} s_1 \\ s_2 \\ s_3 \end{bmatrix} \tag{72}$$

in the feasible set, *i.e.*, for $s_j \in [-0.5,\ 0.5]\text{m}$, which corresponds to the area within the black parallelogram shown in Figure 4. As can be seen in the Figure, the red rectangle representing the set Ω_Δ is strictly inside the parallelogram with at least a 5% margin, thereby satisfying the balancing requirements.

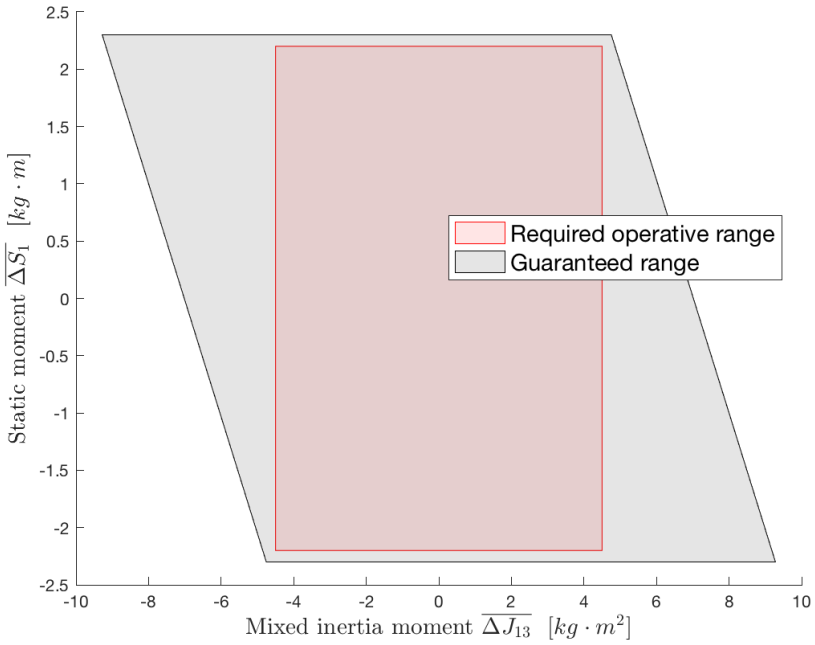

Figure 4 Operative range of the breadboard.

C. Control law tuning

In this section we present the procedure employed to tune the weighting matrices Q and R in the gain matrix (57). The procedure has been performed by requiring that the measured interface loads at the nominal rotor speed ($\Omega = 7.8$ rpm) are below given bounds, specifically $|^r f_{O_1}| < \Delta S_1^{res}\Omega^2 = 0.07$ N and $|^r \tau_{O_2}| < \Delta J_{13}^{res}\Omega^2 = 0.2$ Nm, which correspond to maximum allowed residual unbalances $\Delta S_1^{res} \approx 0.1 kgm$ and $\Delta J_{13}^{res} \approx 0.3 kgm^2$. As explained in Remark 2, the selection of the weighting matrices Q, R in the T-matrix algorithm (51) is based on the trade-off between performance and robustness. For simplicity, we consider $R = I_3$ and $Q = \alpha\, I_4$ with $\alpha := 1/\rho$ a scalar which is the only parameter to tune. Considering the worst-case scenario, namely when $(\Delta S_1, \Delta J_{13}) = \pm(\overline{\Delta S}_1, \overline{\Delta J}_{13})$, different values of α are used in equation (56) and the related suppression levels are plotted in Figure 5, where $|^r \tau_{0_2}| = \sqrt{(^b\tau_{0_2})_c^2 + (^b\tau_{0_2})_s^2}$ and $|f_{0_1}^r| = \sqrt{(^b f_{0_1})_c^2 + (^b f_{0_1})_s^2}$. From the numerical results, $\alpha = 10$ has been chosen, which guarantees a worst-case suppression below the maximum allowed residual unbalance.

Then, a Monte Carlo study has been carried out to assess the robustness of the tuned HC algorithm with respect to uncertainty on the balancing masses (± 0.1 kg) and on their locations (± 0.05 m). More precisely, 10000 samples have been generated and, for each of them, the upper bound on the spectral radius has been evaluated using (63): the maximum bound on $\rho_s(\hat{K}\Delta T)$ found in the tests is 0.0579 (which is much smaller than 1), showing that a high level of robustness is guaranteed with the proposed tuning.

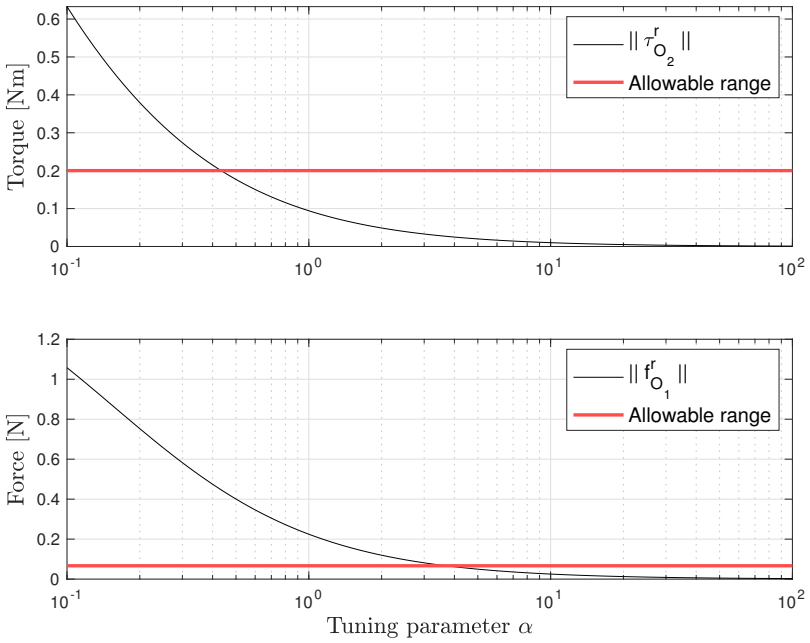

Figure 5 Unbalances suppression with different α.

D. Numerical results

In this section a simulation example is reported with the aim of showing the performance of the proposed ABS combined with HC. For this purpose, a multibody model of the breadboard described in Section V.A, which includes two unbalancing masses (m_1^s = 6kg at $(\bar{x}_1^s, \bar{z}_1^s) = (0.75, 1.46)$m and m_2^s = 4kg at $(\bar{x}_2^s, \bar{z}_2^s) = (-0.75, 0.02)$m), has been developed in Simulink. The control law has been implemented in discrete-time, with an update time of 200 s, which is enough to reach steady-state conditions. Extraction of the harmonics to be used in the T-matrix algorithm is performed through a real-time Fast Fourier Transform (FFT) algorithm that processes the measured signals.

The performance of the control law has been analyzed in two different conditions. In the first one the T-matrix is assumed to be exactly known. The results obtained for this (ideal) case in the discrete-time domain are collected in Table 1.

In this table and in the following ones, "Iteration" corresponds to the discrete-time index; the "Force and Torque amplitude" are computed through the real time FFT algorithm with the balancing masses in the positions reported in the row "Actual"; the rows corresponding to "Computed" report the positions of the masses obtained with the HC at the end of the update-time and to be implemented at the next iteration. On the other hand, the results in continuous-time domain are plotted in Figure 6 and Figure 7.

We can see that a satisfactory vibration suppression is achieved after one update of the control law: the interface force and torque are well below the given thresholds, with the same values for all iterations after the first update (as

Iteration		**0**	**1-2-3-4**
Force amplitude	$[N]$	-1.008	-0.003
Torque amplitude	$[Nm]$	-4.340	-0.007
Actual s_1	$[m]$	0	-0.3251
Actual s_2	$[m]$	0	-0.3583
Actual s_3	$[m]$	0	+0.3583
Computed s_1	$[m]$	-0.3251	-0.3251
Computed s_2	$[m]$	-0.3583	-0.3583
Computed s_3	$[m]$	+0.3583	+0.3583

Table 1 Ideal case results.

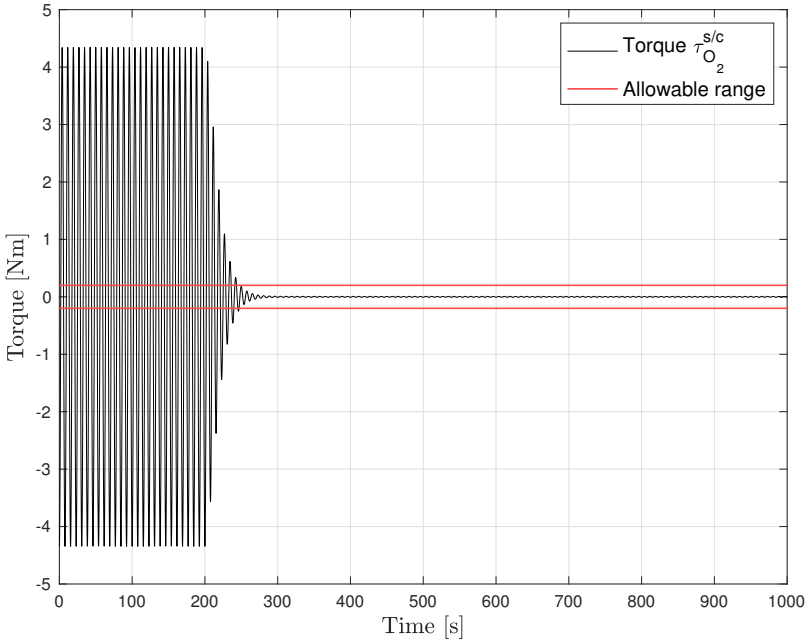

Figure 6 Torque suppression - Nominal case.

expected from equation (54)).

In the second case, the ABS performance is evaluated in a more realistic scenario in which the system is affected by parametric uncertainties and imperfect knowledge of exogenous disturbances, which must be removed from the measured signal before applying the HC algorithm (Remark 7). Besides the already mentioned torque associated with gravity (67), a sinusoidal force of the form ${}^b f_{e_1} = A_e \sin(\omega_e t + \phi_e)$, with $A_e = 0.21$ N, $\phi_e = 1.93$ rad, has been removed from the measured interface force to replicate the disturbance identified on the real platform when rotating at very low speed, a condition in which the force and torque associated with inertial unbalances are very small.[†] A Monte Carlo study (500 simulations) has been carried out with respect to: uncertainty on the unbalancing masses (±0.2 kg) and on

[†]While the root-cause of such a disturbance is probably a combination of several factors, *e.g.*, friction, a small inclination of the structure with respect to the gravity direction, it was found to be almost invariant with respect to the rotating speed but dependent on the specific unbalancing. Hence, in the experimental tests, a model of the disturbance has been identified at low speed at the beginning of each test and then used to compensate the disturbance in the signal measured at the nominal operating speed.

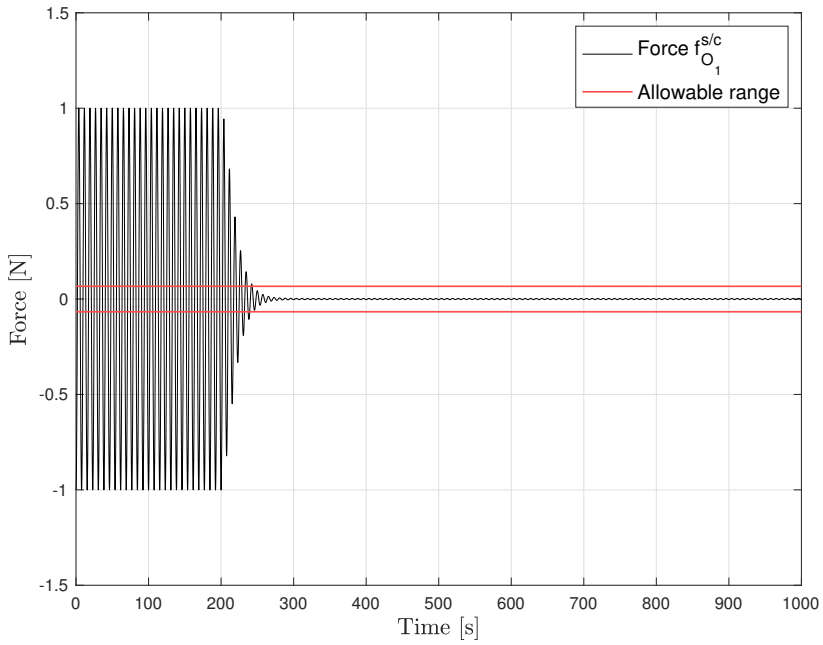

Figure 7 Force suppression - Nominal case.

their locations (±0.1 m);[‡] uncertainty on the amplitude (±0.05 N) and phase (±0.1 rad) of the compensated disturbance force; uncertainty on the ABS components (balancing masses and locations) using the same values considered in the previous section. The most relevant statistics (mean, standard deviation, maximum and minimum values) of the absolute value of the interface loads at the last iteration of the HC algorithm are collected in Table 2, while Figure 8 and Figure 9 depict the corresponding time-domain representations. We can see that a satisfactory suppression is achieved in all the tests, despite the uncertainties.

Statistical parameter	**Force** $[N]$	**Torque** $[Nm]$
Mean	0.003	0.007
Standard Deviation	0.007	0.006
Minimum	0.001	0.001
Maximum	0.029	0.022

Table 2 Statistical properties Monte Carlo simulations.

E. Experimental results

In this section, we present the results obtained by applying the HC algorithm on the breadboard shown in Figure 10. In addition to the breadboard, the experimental setup includes:

- a charge Amplifier (*Kistler Type 5080A*) which receives the signals from the load cells and provides as output suitably amplified analog measurements of the interface force and torque;

[‡]The values of the unbalancing masses are used only for the computation of the gravity torque (67) and are not needed for the on-orbit case (see Remark 7).

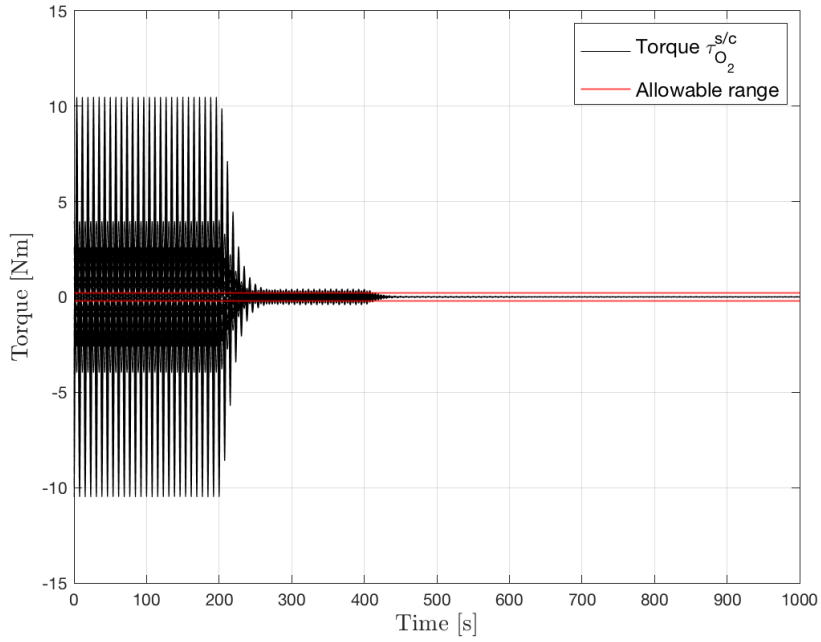

Figure 8 Torque suppression - Monte Carlo analysis.

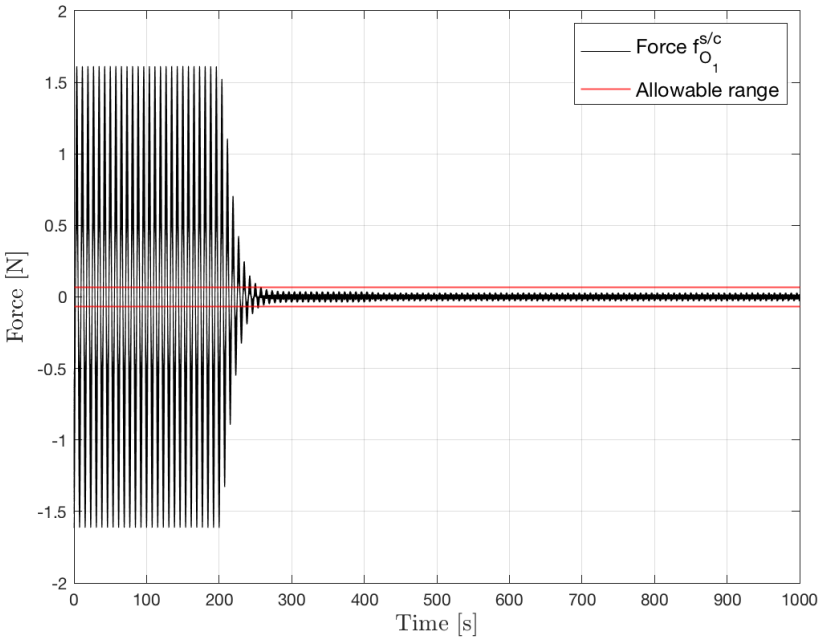

Figure 9 Force suppression - Monte Carlo analysis.

- a data acquisition board (*National Instruments USB-6003*) which takes as input the amplified signals;
- a laptop computer which receives the output of the acquisition board, runs the HC algorithm and sends the commands to the linear actuators; it is also used to set the speed of the rotor.

A schematic view of the overall setup is shown in Figure 11. The balancing tests reported in the following have been

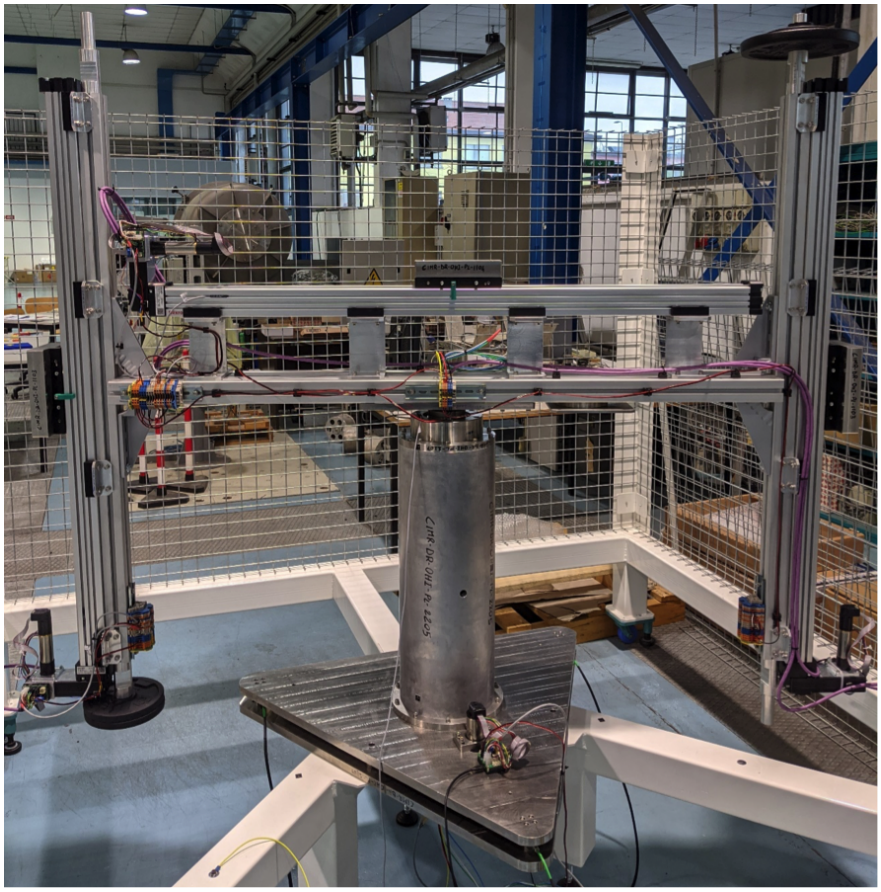

Figure 10 Breadboard used in the experiments.

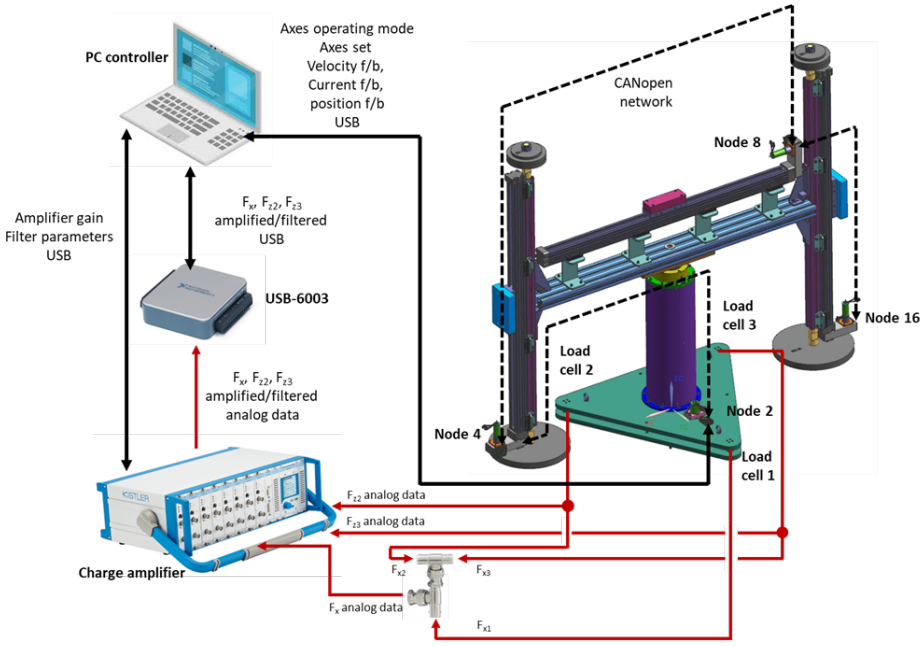

Figure 11 Test setup scheme.

carried out at the nominal rotor speed ($\Omega = 7.8$ rpm) through the following steps:[§]

1) a set of unbalance masses are mounted on the rotor;
2) data are logged for 300 s using the USB-6003 acquisition board;
3) the discrete FFT is applied to the logged signal to evaluate the interface loads amplitude at the rotating frequency of the rotor;
4) the target positions of the balancing masses are computed through the HC algorithm;
5) an operator checks the algorithm outputs. If the positions are feasible, the operator sends them to the actuators;
6) the actuators receive the commands and we wait until the target positions are reached;
7) the steps 2-3 are repeated to check that the system is balanced. If not, the steps 4-6 are repeated until the system is balanced.

Remark 8 The choice of implementing the HC algorithm with a human-in-the-loop approach is motivated by the expected on-orbit procedures in which a ground operator will have to assess, for safety reasons, the correctness of the computed positions of the masses, due to the criticality of balancing operations. It is worth mentioning that a limited amount of iterations is expected. ⌟

In the following, three experiments with different unbalancing masses and with increasing complexity are presented:

- a *static unbalance compensation* test, in which only the central balancing mass is used;
- a *dynamic unbalance compensation* test, in which only the vertical balancing masses are used;
- *a combined static and dynamic unbalances compensation* test in which all the balancing masses are used.

1. Static unbalance compensation

The first balancing test involves $m_1^s = 1.051$kg at $(\bar{x}_1^s, \bar{z}_1^s) = (0.75, 1.46)$m and $m_2^s = 1.046$kg at $(\bar{x}_2^s, \bar{z}_2^s) = (0.75, 0.02)$m. To compensate for the resulting static unbalance ($\Delta S_1 = 1.57$ kgm), the ideal position of the balancing mass m_1 should be

$$s_1 = -\frac{\Delta S_1}{m_1} = -0.34\text{m}. \tag{73}$$

The data related to this test are reported in Table 3. By inspecting the table, the slight difference in terms of the computed position (last row of Table 3, second iteration) with respect to the ideal position of the balancing mass (equation (73)) is likely due to the intrinsic unbalance of the structure and to a slightly erroneous compensation of the disturbance $f_{e_1}^b$. Thanks to the second iteration of the HC algorithm, the measured interface load $|f_{O_1}^r|$ is reduced to 0.037 N, which is below the required threshold (0.07N).

[§]As mentioned before, at the beginning of each test a preliminary test at low speed ($0.5RPM$) is performed with the aim of identifying possible disturbances, not related to inertial unbalances, to be removed from the measured signals before applying the HC algorithm.

Iteration		**0**	**1**	**2**
Force amplitude	$[N]$	-1.035	-0.071	-0.037
Static unbalance	$[kgm]$	1.551	0.106	0.056
Actual s_1	$[m]$	0	-0.3101	-0.3130
Computed s_1	$[m]$	-0.3101	-0.3130	-0.3169

Table 3 Static unbalance compensation test.

2. Dynamic unbalance compensation

The second balancing test involves $m_1^s = 5.047$kg at $(\bar{x}_1^s, \bar{z}_1^s) = (0.75, 1.46)$m and $m_2^s = 5.170$kg at $(\bar{x}_2^s, \bar{z}_2^s) = (-0.75, 0.02)$m. To compensate for the resulting dynamic unbalance ($\Delta J_{13} = -5.45\,\text{kgm}^2$), the ideal position of the balancing masses m_2 and m_3 should be

$$s_2 = -s_3 = \frac{\Delta J_{13}}{m_2 \bar{x}_2} = -0.38\text{m}. \tag{74}$$

As done for the first experiment, the data related to this test are reported in Table 4. In this case only one iteration of the HC algorithm is required. Indeed, the ideal and commanded positions of the balancing masses (equation (74)) are almost coincident after only one iteration and the measured interface load $|\tau_{O_2}^r|$ is reduced to 0.152 Nm, which is below the required threshold $(0.2Nm)$.

Iteration		**0**	**1**
Torque amplitude	$[Nm]$	-3.657	-0.152
Dynamic unbalance	$[kgm^2]$	-5.482	-0.228
Actual s_2	$[m]$	0	-0.3810
Actual s_3	$[m]$	0	+0.3810
Computed s_2	$[m]$	-0.3810	-0.3943
Computed s_3	$[m]$	+0.3810	+0.3943

Table 4 Dynamic unbalance compensation test.

3. Combined unbalance compensation

The last balancing test involves $m_1^s = 6.193$kg at $(\bar{x}_1^s, \bar{z}_1^s) = (0.75, 1.46)$m and $m_2^s = 4.185$kg at $(\bar{x}_2^s, \bar{z}_2^s) = (-0.75, 0.02)$m. To compensate for the resulting unbalances ($\Delta S_1 = 1.51\,\text{kgm}$ and $\Delta J_{13} = -6.7\,\text{kgm}^2$), the nominal position of the balancing masses m_1, m_2 and m_3 should be

$$s_1 = -\frac{\Delta S_1}{m_1} = -0.33\text{m},\ s_2 = -s_3 = \frac{\Delta J_{13} - m_1 \bar{z}_1 s_1}{m_2 \bar{x}_2} = -0.37\text{m}. \tag{75}$$

The data related to this test are reported in Table 5. Also in this case only one iteration of the HC algorithm is required to reduce the measured interface loads below the required thresholds and the values of the commanded positions are close to the expected ones.

Iteration		**0**	**1**
Force amplitude	$[N]$	-1.086	-0.001
Torque amplitude	$[Nm]$	-4.282	-0.029
Static unbalance	$[kgm]$	1.628	0.002
Dynamic unbalance	$[kgm^2]$	-6.419	-0.0435
Actual s_1	$[m]$	0	-0.3328
Actual s_2	$[m]$	0	-0.3539
Actual s_3	$[m]$	0	0.3539
Computed s_1	$[m]$	-0.3328	-0.3329
Computed s_2	$[m]$	-0.3539	-0.3540
Computed s_3	$[m]$	0.3539	0.3540

Table 5 Combined unbalance compensation test.

VI. CONCLUSIONS

In this work, we presented the results of a pre-development activity aimed at the maturation of an ABS for the CIMR mission. Specifically, we proposed a system made of actuated movable masses and suitable sensors, combined with a controller based on harmonic control ideas, to mitigate the effect associated with inertial asymmetries of rotating payloads. The effectiveness of the proposed design has been evaluated both in simulation as well as through experiments on a dedicated breadboard. The results showed that the system is capable of reducing the force and torque induced by the unbalance at the interface between the fixed and the rotating part within predefined bounds, even in the presence of imperfect knowledge of the system parameters. Future work will be devoted to validating numerically the proposed design in a representative simulation environment, accounting for antenna flexibility effects, orbital dynamics and perturbations and to further studying the interplay between the harmonic controller for active balancing and the attitude controller of the spacecraft, for which some preliminary results are available in [10]. Another interesting research direction is the development of a combined control architecture for both attitude control and balancing.

Funding Sources

This work was partially supported by CIMR-CN-OHI-SY-0003, iss. 1, dated 17/05/2019 from Thales Alenia Space Italy and The European Space Agency.

References

[1] Entekhabi, D., and Njoku, E. G., "The Soil Moisture Active Passive (SMAP) Mission," *Proceedings of the IEEE*, Vol. 98, No. 5, 2010, pp. 704–716. https://doi.org/10.1109/JPROC.2010.2043918.

[2] Vanin, F., Laberinti, P., Donlon, C., Fiorelli, B., Barat, I., Sole, M. P., Palladino, M., Eggers, P., Rudolph, T., and Galeazzi, C., "Copernicus Imaging Microwave Radiometer (CIMR): System Aspects and Technological Challenges," *IGARSS 2020 - 2020*

IEEE International Geoscience and Remote Sensing Symposium, 2020, pp. 6535–6538. https://doi.org/10.1109/IGARSS39084.2020.9324259.

[3] Gonçalo, R., "Deployable Structures Activities at the European Space Agency's Structures Section," *Proceeding of ECSSMET 2016-14th European Conference on Spacecraft Structures, Materials and Environmental Testing, Toulouse, France*, 2016.

[4] Mobrem, M., Keay, E., Marks, G. C., and Slimko, E., "Development of the Large Aperture Reflector/Boom Assembly for the SMAP Spacecraft," 2012.

[5] Donlon, C., "Mission Requirements document: Copernicus Imaging Microwave Radiometer," Tech. rep., ESA, 2019.

[6] Alvarez-Salazar, O. S., Adams, D., Milman, M., Nayeri, R., Ploen, S., Sievers, L., Slimko, E., and Stephenson, R., "Pointing Architecture of SMAP's Large Spinning Antenna," *AIAA Guidance, Navigation, and Control (GNC) Conference*, 2013. https://doi.org/10.2514/6.2013-4560.

[7] Qiuxiao, W., and Fei, W., "A new vibration mechanism of balancing machine for satellite-borne spinning rotors," *Chinese Journal of Aeronautics*, Vol. 27, No. 5, 2014, pp. 1318 – 1326. https://doi.org/https://doi.org/10.1016/j.cja.2014.08.001.

[8] Meraglia, S., Invernizzi, D., and Lovera, M., "Active Balancing Systems For Rotating Orbital Devices," *25th Conference of the Italian Association of Aeronautics and Astronautics*, 2019, pp. 369–376.

[9] Valsecchi, L., Apollonio, P., Molina, M., Olivier, M., Bernelli-Zazzera, F., Lovera, M., and Bittanti, S., "Design and testing of an active damping system for the reduction of vibrations induced by a rotating device on the ISS," *54th Int. Astronautical Congress, Bremen, Germany*, 2003.

[10] Invernizzi, D., "Modeling and Attitude Control of Spacecraft With an Unbalanced Rotating Device," *IEEE Control Systems Letters*, Vol. 7, 2023, pp. 466–471. https://doi.org/10.1109/LCSYS.2022.3187877.

[11] Friedmann, P., and Millott, T. A., "Vibration reduction in rotorcraft using active control: A comparison of various approaches," *Journal of Guidance, Control, and Dynamics*, Vol. 18, 1995, pp. 664–673. https://doi.org/10.2514/3.21445.

[12] Shaw, J., and Albion, N., "Active Control of the Helicopter Rotor for Vibration Reduction," *Journal of the American Helicopter Society*, Vol. 26, No. 3, 1981, pp. 32–39.

[13] Badlani, M., Kleinhenz, W., and Hsiao, C., "On vibration of rotating shafts," *Mechanism and Machine Theory*, Vol. 13, No. 5, 1978, pp. 555 – 564. https://doi.org/https://doi.org/10.1016/0094-114X(78)90008-3.

[14] Bishop, E. D., and Parkinson, R., "On the Use of Balancing Machines for Flexible Rotors," *Journal of Engineering for Industry*, Vol. 94, 1972, p. 561. https://doi.org/10.1115/1.3428193.

[15] Zhou, S., and Shi, J., "Active Balancing and Vibration Control of Rotating Machinery: A Survey," *The Shock and Vibration Digest*, Vol. 33, 2001, pp. 361–371. https://doi.org/10.1177/058310240103300501.

[16] Welsh, W., "Evolution of Active Vibration Control Technology," *Proceedings of the AHS 4th Decennium Specialist's Conference on Aeromechanics*, 2004.

[17] Patt, D., Liu, L., Chandrasekar, J., Berstein, D. S., and Friedmann, P., "Higher-Harmonic-Control Algorithm for Helicopter Vibration Reduction Revisited," *Journal of Guidance Control and Dynamics*, Vol. 28, 2005. https://doi.org/10.2514/1.9345.

[18] Lovera, M., Colaneri, P., Malpica, C., and Celi, R., "Closed-Loop Aeromechanical Stability of Hingeless Rotor Helicopters with Higher Harmonic Control," *Journal Of Guidance, Control and Dynamics*, Vol. 29, No. 1, 2006, pp. 179–189. https://doi.org/10.2514/1.7949.

[19] Wereley, N. M., and Hall, S. R., "Frequency response of linear time periodic systems," *29th IEEE Conference on Decision and Control*, Vol. 6, 1990, pp. 3650–3655. https://doi.org/10.1109/CDC.1990.203516.

[20] Chandrasekar, J., Liu, L., Patt, D., Friedmann, P., and Bernstein, D. S., "Adaptive Harmonic Steady-State Control for Disturbance Rejection," *IEEE Transactions on Control Systems Technology*, Vol. 14, 2006, pp. 993 – 1007. https://doi.org/10.1109/TCST.2006.880185.

[21] Lovera, M., Colaneri, P., Malpica, C., and Celi, R., "Discrete-time, closed-loop aeromechanical stability analysis of helicopters with Higher Harmonic Control," *Journal of Guidance, Control and Dynamics*, Vol. 30, 2007, pp. 1249–1260.

[22] Zhou, J., and Hagiwara, T., "H_2 and H_∞ norm computations of linear continuous-time periodic systems via the skew analysis of frequency response operators," *Automatica*, Vol. 38, 2002, pp. 1381–1387. https://doi.org/10.1016/S0005-1098(02)00038-9.